Construction and Building Materials 356 (2022) 129227

Contents lists available at ScienceDirect

Construction and Building Materials

journal homepage: www.elsevier.com/locate/conbuildmat

Explainable machine learning models for predicting the axial compression capacity of concrete filled steel tubular columns

Celal Cakiroglu [a,*], Kamrul Islam [b], Gebrail Bekdaş [c], Umit Isikdag [d], Sujith Mangalathu [e]

[a] Department of Civil Engineering, Turkish-German University, Istanbul 34820, Turkey
[b] Department of Civil, Geological and Mining Engineering, Polytechnique Montréal, Canada
[c] Department of Civil Engineering, Istanbul University-Cerrahpaşa, Istanbul 34320, Turkey
[d] Department of Informatics, Mimar Sinan Fine Arts University, Istanbul 34427, Turkey
[e] Data Analytics Division, Mangalathu, Mylamkulam, Puthoor PO, Kollam, Kerala, 691507, India

ARTICLE INFO

Keywords:
Explainable machine learning
Artificial intelligence (AI)
Composite column
Compressive capacity
Resistance factor

ABSTRACT

Concrete-filled steel tubular (CFST) columns have been popular in the construction industry due to enhanced mechanical properties such as higher strength and ductility, higher seismic resistance, and aesthetics. Extensive experimental, numerical and analytical studies have been conducted in the past few decades to assess the structural response of CFST columns under various loading conditions. However, there is still uncertainty in predicting the capacity of CFST columns, and most of the current codes are conservative. In this paper, data-driven machine learning (ML) models have been developed to predict the axial compression capacity of rectangular CFST columns. An extensive database of 719 experiments was collected from literature and is randomly used to train, test, and validate the ML models. Seven ML models, namely lasso regression, random forest, Adaptive Boosting (AdaBoost), Gradient Boosting Machine (GBM), Light Gradient Boosting Machine (LightGBM), Extreme Gradient Boosting (XGBoost), and Categorical Gradient Boosting (CatBoost), are evaluated to predict the compression capacity of CFST stub columns under axial load. The performance of the different ML models in predicting the compressive strength of CFST columns is compared by different code equations prevalent in different parts of the world. It is found that LightGBM and CatBoost models performed better with an accuracy of 97.9% and 98.3%, respectively, compared to the existing design codes in predicting the capacity of CFST columns. Feature importance analyses and SHapley Additive exPlanations (SHAP) explain the ML model performances and make the developed models interpretable. Resistance factor is determined using the best performing ML model for compressive strength prediction of CFST stub columns following AISC 360–16 code provision.

1. Introduction

Concrete-filled steel tubular (CFST) columns are widely used high-performance composite columns exhibiting higher strength, ductility, stiffness, and large energy absorption capacity when compared to reinforced concrete or steel columns [1–6]. CFST columns combine the best properties of concrete and steel simultaneously. On the one hand, the steel tube provides confinement of the core, causing the concrete to behave in a tri-axial stress state, increasing the strength and ductility. On the other hand, the concrete core helps significantly reduce the premature local buckling of the steel tube [7,8]. Moreover, CFST columns reduce the construction time and cost as no form-works are needed. Therefore, CFST columns have gained worldwide popularity for constructing buildings and bridges in non-seismic and high seismic zones. The favorable effect of using CFST members on the buckling behavior can also be seen in Fig. 1, where the buckling mode shapes are visualized for a hollow steel tube (Fig. 1b) and a concrete-filled steel tube (Fig. 1c).

CFST columns, due to their multiple benefits, have found their way into various construction projects worldwide. Much research efforts have been given for their development through experimental and numerical studies [9–10]. Their uses include the columns of the Taipei 101 skyscraper [11], and various other cases such as chords in composite arch bridges [12], special moment frames [13], bridge piers [14], the two union square building in Seattle, Washington, 3 Houston Center in Houston, Texas, the Capella Tower in Minneapolis, Seattle Municipal

* Corresponding author.
E-mail addresses: cakiroglu@tau.edu.tr (C. Cakiroglu), kamrul.islam@polymtl.ca (K. Islam), bekdas@iuc.edu.tr (G. Bekdaş), umit.isikdag@msgsu.edu.tr (U. Isikdag), sujithmss@gatech.edu (S. Mangalathu).

https://doi.org/10.1016/j.conbuildmat.2022.129227
Received 2 June 2022; Received in revised form 12 September 2022; Accepted 16 September 2022
Available online 2 October 2022

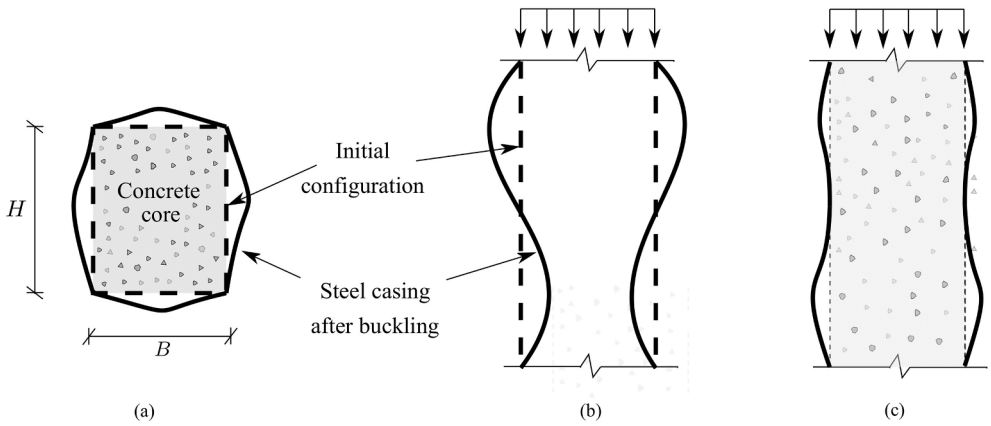

Fig. 1. Buckling mode shapes of a) concrete-filled cross-section, b) steel casing without concrete infill, c) concrete-filled steel tube.

Table 1
Code and model equation limitations on material strength in CFST columns.

Design code	Steel strength (MPa)	Concrete strength (MPa)
AISC 360–16	$235 \leq f_y \leq 525$	$21 \leq f_c' \leq 69$
EC 4	$235 \leq f_y \leq 460$	$20 \leq f_c' \leq 50$
AS-5100.6	$230 \leq f_y \leq 400$	$25 \leq f_c' \leq 65$
Wang et al.[54]	$194 \leq f_y \leq 835$	$13 \leq f_c' \leq 164$

Tower in Seattle, Washington. Since the first experimental program was conducted on CFST columns in late 1950 [15], extensive experimental research works have been performed on the response of CFST columns subjected to compression, tension, flexure, combined compression and bending moment, and torsion [16–33]. Tao et al. [34,35], Leon et al. [36], Hajjar et al. [37], Lai et al. [38,39], Lai and Varma [40,41], Thai et al. [42], Yu et al [43,44] compiled comprehensive experimental databases on CFST columns, beams, frames and systems. Those databases consist of compact, non-compact, and slender CFST members with a

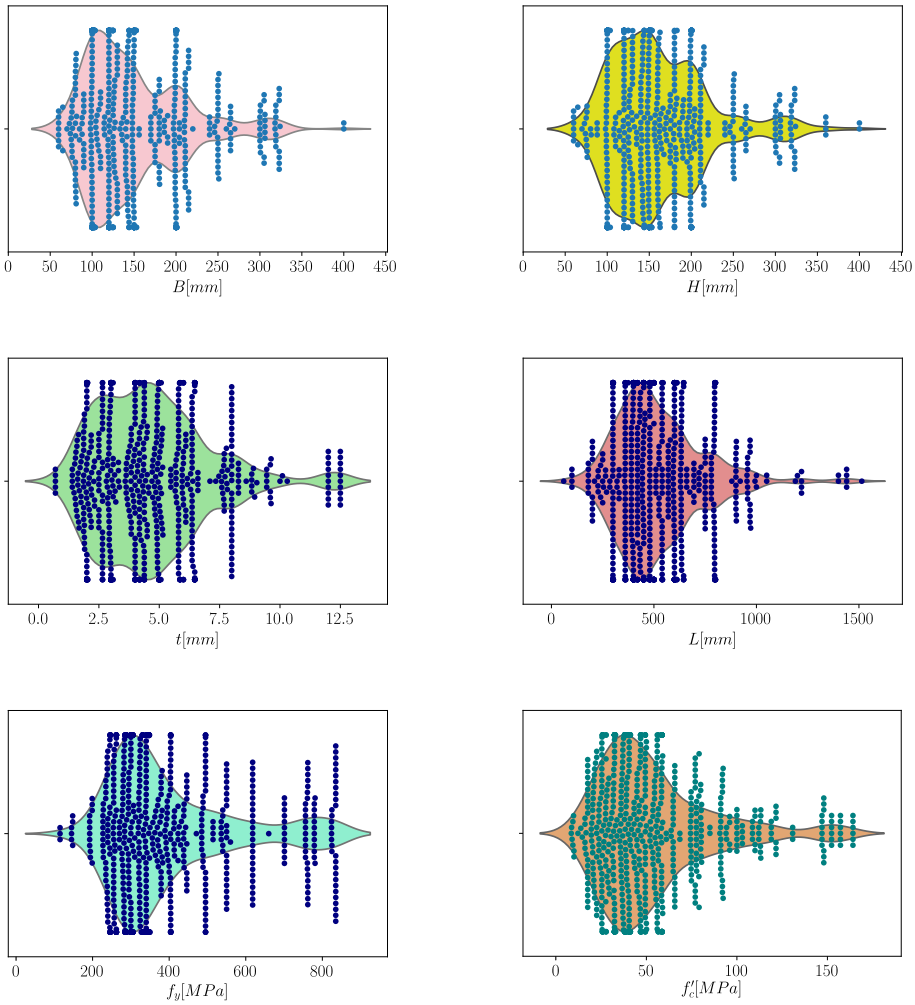

Fig. 2. Violin plots with swarm plot overlay showing the distribution of the variables.

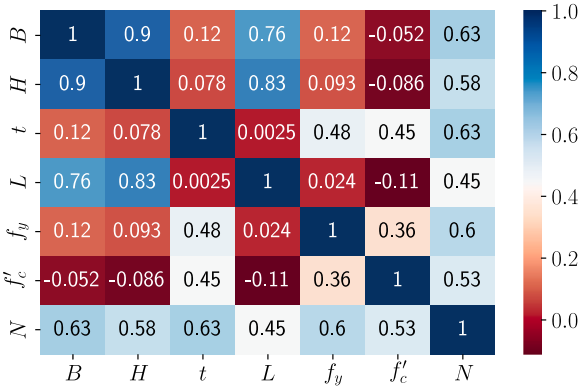

Fig. 3. Pearson correlation between the design variables and the axial load carrying capacity.

wide variety of geometric and material properties. The outcomes of those research indicate that the structural response of CFST columns depend on the size and shape of the steel section, the fabrication process of the steel section, the strength of infilled materials used, and the loading condition.

The available design codes, such as the American Institute of Steel Construction (AISC 360-16)[45], Eurocode 4 (EC4) [46], and Australian Steel Standard (AS 5100) [47], provide excellent design guidelines for different types of CFST columns. However, most of the current codes impose restrictions on the use of high-strength materials in CFST columns. Material limits for rectangular CFST columns are presented in Table 1. It can be seen from Table 1 that high strength materials are still prohibited in most of the design codes, despite significant experimental tests and numerical parametric studies that have been carried out on CFST columns utilizing high strength steel and concrete materials in the last two decades [1–3,5,40,48–54]. Lai and Varma (2015) [40] prepared an extensive database of high-strength rectangular CFST columns and proposed new design equations and a resistance factor (ϕ) for calculating the cross-sectional strength through an extensive finite element (FE) parametric study. They also suggested effective stress-strain relationships for the steel tube and concrete infill. It should be noted that all the previous studies have highlighted the conservative nature of code-predicted equations. Although FE models can simulate the response of CFST columns with high precision, developing benchmarked FE models are cumbersome and computationally extensive. Therefore, it is important to develop accurate and robust data-driven models to predict the capacity of CFST columns.

Researchers have proposed several ML techniques to aid in the capacity estimation and progressive collapse assessment, failure mode prediction, design, and the determination of structural demands [55–64,83,84]. Among the areas of structural engineering where machine learning models have been applied, failure mode recognition of circular reinforced concrete bridge columns [65], vulnerability assessment of bridges against fire [66], rapid prediction of earthquake-induced building damage [67], failure mode classification and shear strength prediction of reinforced concrete beams, beam-column joints and shear walls [68–70,84] can be counted. Past studies also utilized the power of data-driven models to predict the capacity of CFST columns. Tran et al. (2019, 2020) [71,72] developed an extensive database of CFST rectangular and circular columns and used ANN to predict the

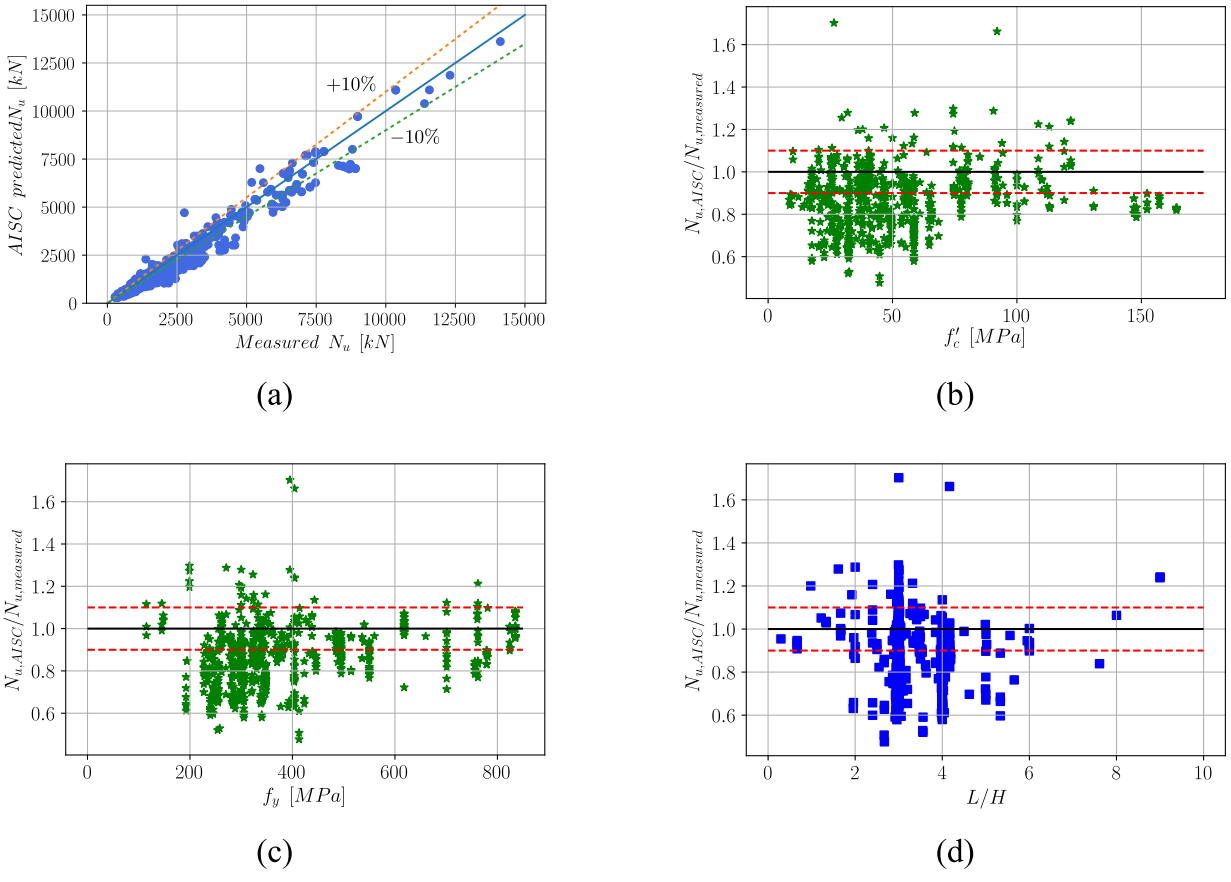

Fig. 4. Correlation between measured and AISC 360–16 predicted axial load capacities.

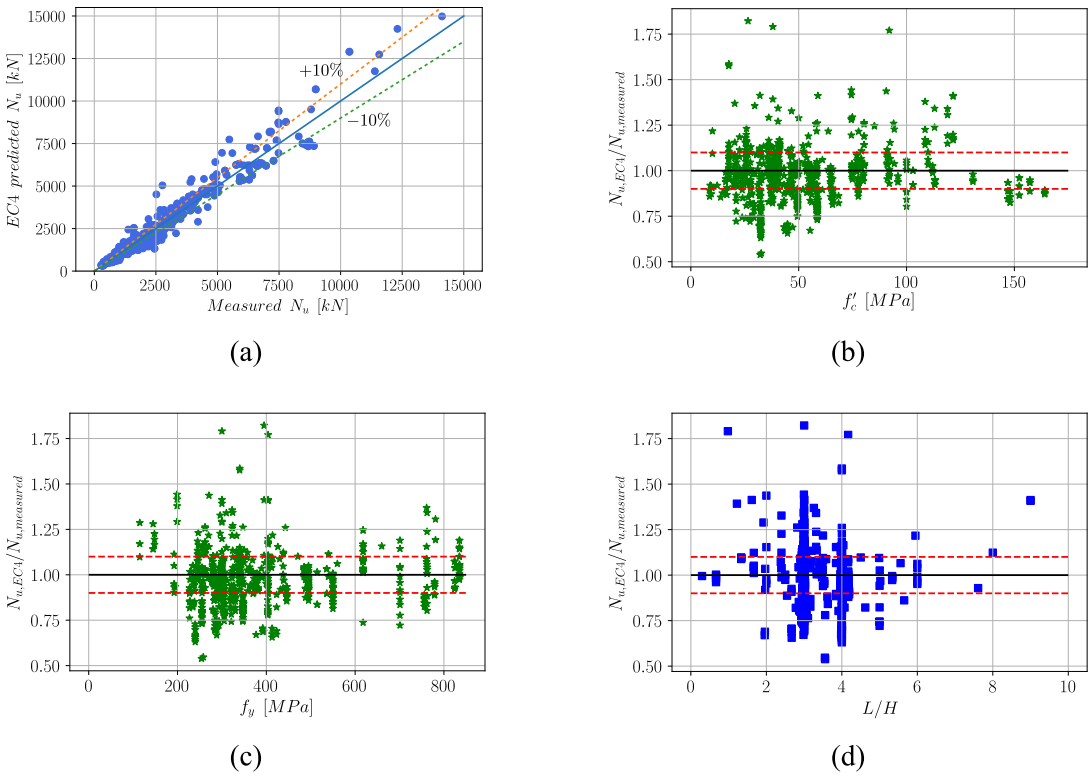

Fig. 5. Correlation between measured and EC4 predicted axial load capacities.

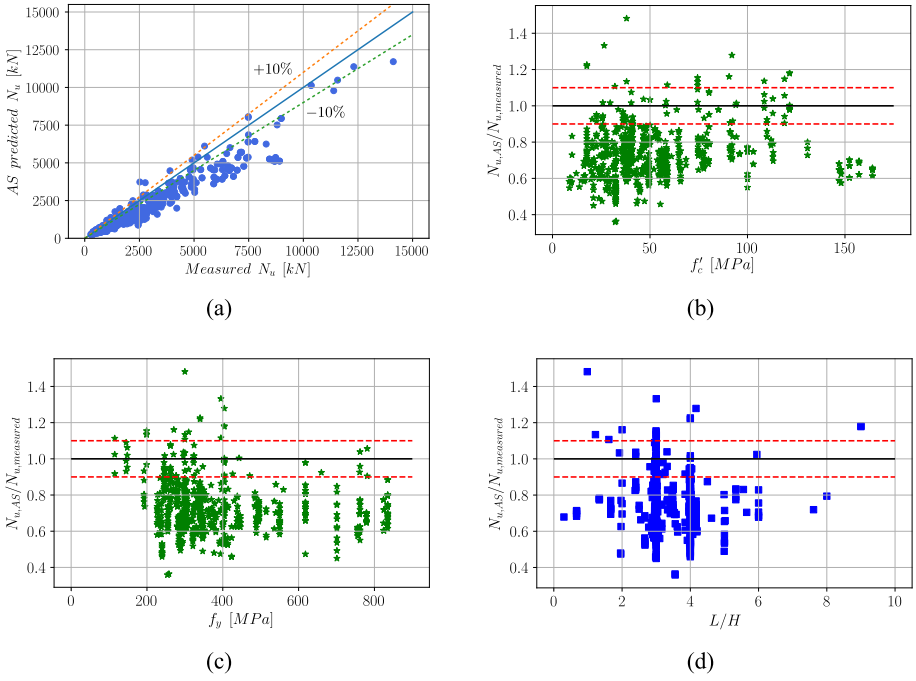

Fig. 6. Correlation between measured and AS-5100.6 predicted axial load capacities.

ultimate strength of CFST columns. Zarringol et al. (2020) [73] also used ANN-based model to predict the capacity of rectangular and circular CFST columns subjected to concentric and eccentric loading. Naser et al. (2021) [63] utilized 3103 test results of CFST columns to develop data-driven models using genetic algorithm (GA) and gene expression programming (GEP). All the studies above reported high precision of the predictive models compared to the code-predicted compressive capacity. However, these studies are limited to using ML methods than the explanation of the predicted value. Moreover, those studies focused on traditional single learning algorithms for predicting the outcomes. Several recent studies have developed data-driven models using an extensive database to estimate different CFST columns' capacity [74–75]. However, the developed models are "black box" in nature, and they are unable to explain the underlying physics of the problem,

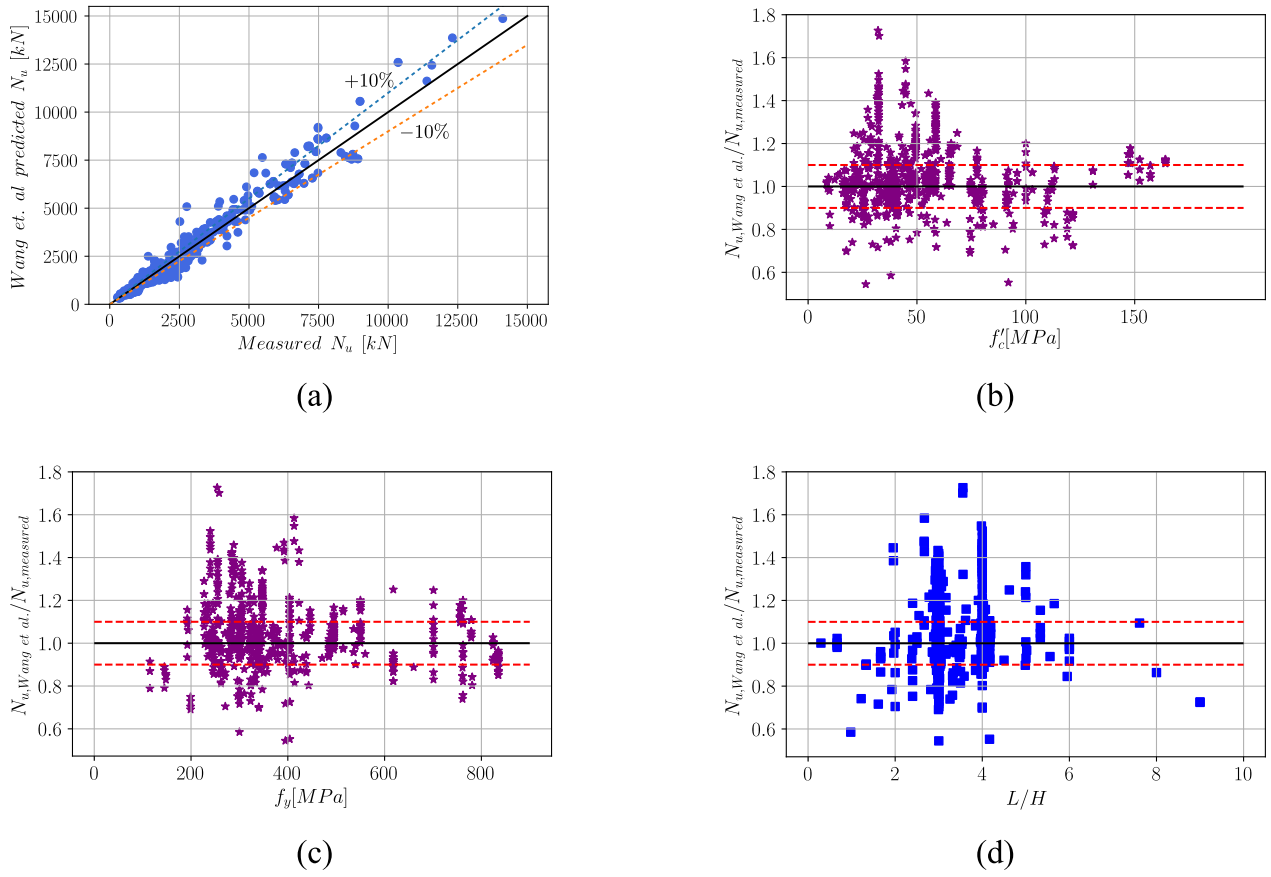

Fig. 7. Correlation between axial load capacities measured and predicted by Wang et al. [54].

although they showed very high accuracy against test datasets. It should be noted here that very high predictive capacity and accuracy are not enough to make an ML model reliable. The developed ML models should be sufficiently explainable and interpretable. Hence the current study focuses on developing explainable ML models to predict the compressive capacity of CFST short columns. Moreover, there is a research gap of systematic comparison between different ensemble ML models to predict the capacity of composite columns. Here the authors have only focused on rectangular CFST stub columns to predict the cross-sectional resistance. The intermediate and long columns are not included in the database as those columns' behavior depends on geometric and material properties and support conditions, loading history, residual stress pattern, and geometric imperfection [51–53,76–77]. Previous studies ignored those input parameters while developing the data-driven models for intermediate and long CFST columns [63,71–75].

The objective of this study was to determine the cross-sectional resistance of rectangular CFST stub columns in a more accurate way to overcome the inefficiencies of the design standards and various prediction equations available in the literature. Since these equations are limited to a specific range of geometric dimensions and material strength, their usage outside of these ranges is not recommended. Therefore, it is crucial to utilize modern machine learning algorithms to obtain methods of prediction that can be used for a wider range of design variables. A novelty of the current study is that the proposed machine learning models are not limited to parameter ranges defined in the existing codes. They are applicable to a wider range of datasets that can accurately capture the axial load carrying capacity beyond the current code limits. To show the effectiveness of machine learning in predicting the axial load carrying capacity, the most commonly used design equations are applied to the collected database of experiments, and their performances are compared to predictions made by machine learning algorithms. In the current study, a wide range of CFST stub-column test data having diversification in specimen results are used to develop the data-driven models. Furthermore, the present study is the first one in the literature that includes interpretable machine learning models developed for predicting the capacity of CFST columns as most of the traditional machine learning models are black-box in nature. This study explains the complex input–output relation of the developed ML models through feature importance analyses and SHAP algorithm.

2. Overview of existing design codes and formulations

The AISC 360-16 [45] code includes three different equations for the prediction of N_u depending on the cross-section slenderness defined as the side length to wall thickness ratio. The cross-sections are categorized as compact, non-compact, and slender, depending on the λ ratio. A cross-section is categorized as compact if $\lambda \le \lambda_p = 2.26\sqrt{E_s/f_y}$, as non-compact if $2.26\sqrt{E_s/f_y} < \lambda \le 3.0\sqrt{E_s/f_y}$ and as slender if $\lambda_r = 3.0\sqrt{E_s/f_y} < \lambda$. The calculation of N_u according to AISC 360-16 for all three cases can be done using Eqs. (1) to (3) where E_s is the elasticity modulus of steel and A_s and A_c are the cross-sectional areas of the steel casing and the concrete core, respectively.

$$Compact: P_{u,c} = A_s f_y + 0.85 f'_c A_c \tag{1}$$

$$Non-compact: P_{u,nc} = P_{u,c} - \frac{P_{u,c} - \left(A_s f_y + 0.7 f'_c A_c\right)}{\left(\lambda_r - \lambda_p\right)^2}\left(\lambda - \lambda_p\right)^2 \tag{2}$$

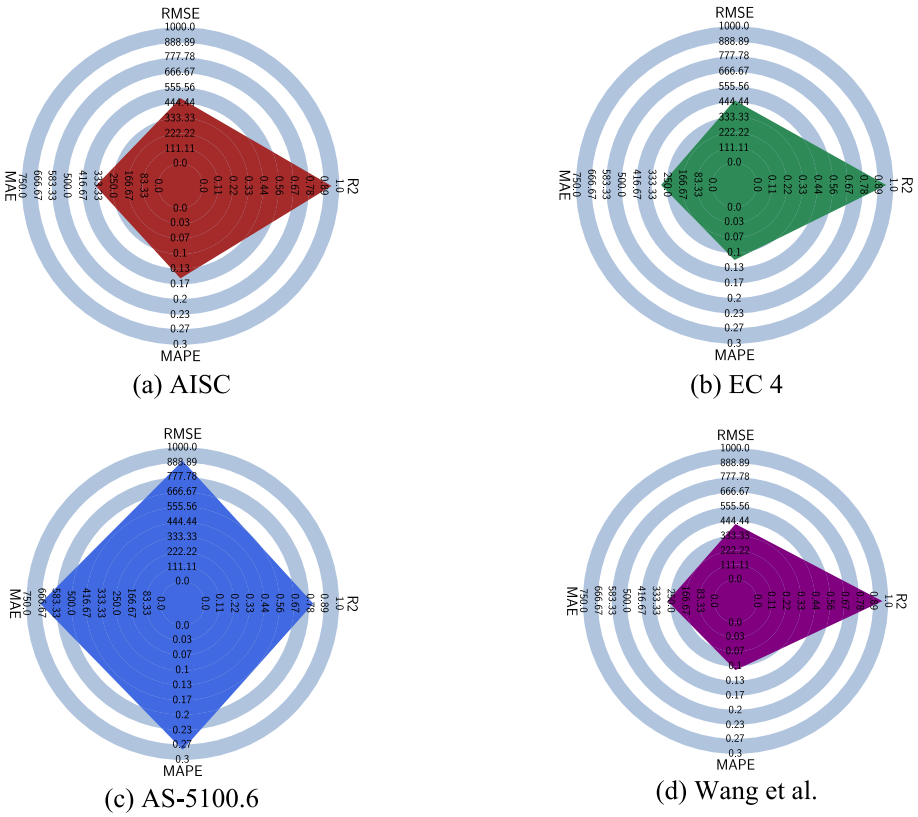

Fig. 8. Radar charts of accuracy metrics for a) AISC 360–16, b) EC4, c) AS-5100.6, d) Wang et al. [54]

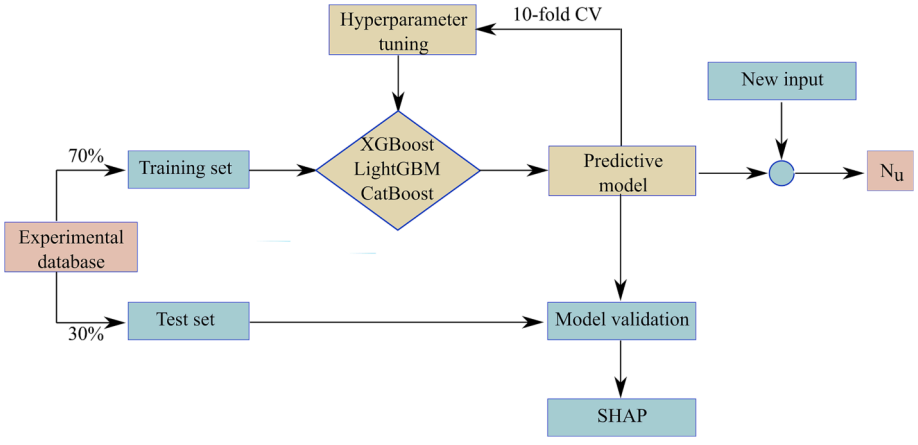

Fig. 9. Ensemble learning flowchart.

$$Slender: P_{u,s} = A_s\frac{9E_s}{\lambda^2} + 0.7f_c^{'}A_c \tag{3}$$

According to Eurocode 4 [46], for rectangular cross-sections N_u is calculated as in Eq. (4).

$$N_u = f_yA_s + f_c^{'}A_c \tag{4}$$

According to the Australian code AS-5100.6 [47], for rectangular cross-sections N_u is calculated as in Eq. (5).

$$N_u = 0.6f_yA_s + 0.9f_c^{'}A_c \tag{5}$$

Eqs. (6) to (10) show the methodology pertaining to CFST columns with rectangular cross-section developed by Wang et al. [54] for calculating N_u.

$$N_u = N_s + N_c \tag{6}$$

$$N_s = \eta_s f_y A_s, N_c = \eta_c f_c^{'} A_c \tag{7}$$

$$\eta_s = 0.91 + 7.31\cdot10^{-5}f_y - \left(1.28\cdot10^{-6} + 2.26\cdot10^{-8}f_y\right)\left(\frac{D^{'}}{t}\right)^2 \tag{8}$$

$$\eta_c = 0.98 + 29.5(f_y)^{-0.48}k_s^{0.2}\left(\frac{tf_y}{D^{'}f_c^{'}}\right)^{1.3} \tag{9}$$

$$k_s = \frac{1}{3}\left(\frac{B-2t}{H-2t}\right)^2 \tag{10}$$

In Eqs. (6) to (10), η_s and η_c model the effects of confinement on the

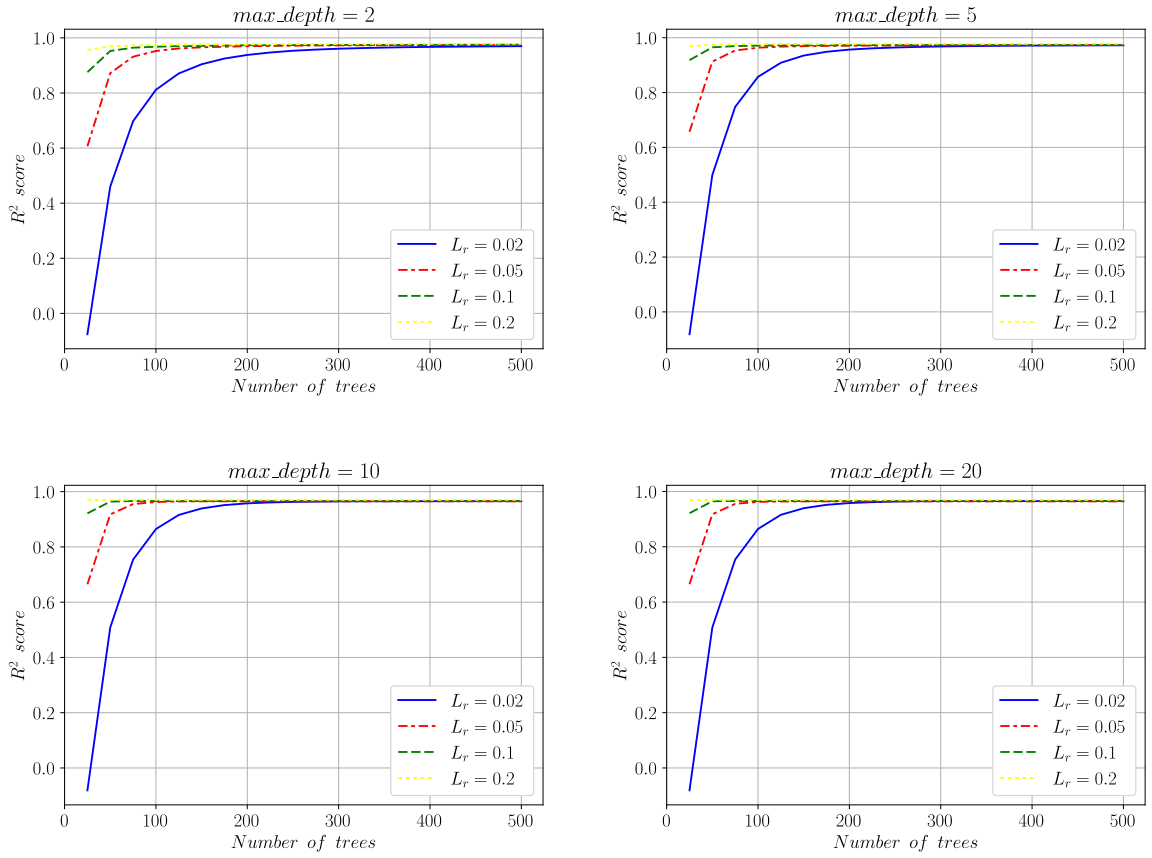

Fig. 10. XGBoost parameter tuning.

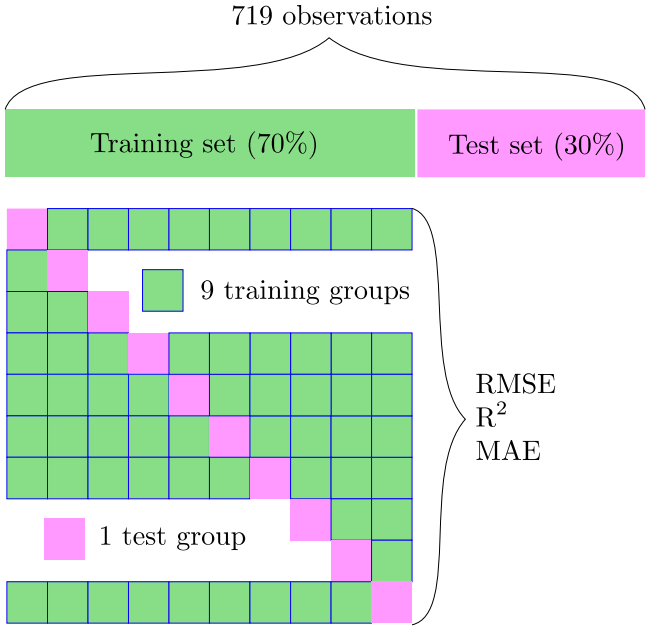

Fig. 11. 10-fold Cross-validation of the training set.

steel and concrete parts, respectively whereas k_s models the lack of concrete confinement due to the rectangular shape of the cross-section. The equivalent diameter is calculated as$D' = \sqrt{B^2 + H^2}$.

3. Employed databases and the statistical summary of the data

A comprehensive database consisting of experimental studies spanning five decades was used in this study to generate a database of 719 samples of rectangular CFST column dimensions and corresponding axial load-carrying capacities under concentric loading. The design variables in this experimental dataset are the side lengths of the rectangular cross-section (B,H), the steel casing wall thickness (t), the length of the specimen (L), the yield stress of steel (f_y) and the compressive strength of the concrete (f_c'). All experiments included in the database satisfy the $\frac{L}{H} \leq 6$ requirement such that they can be classified as stub columns [40]. It should be noted that ML models are fully data-driven, and the model prediction performance largely depends on the quality and quantity of the datasets used to train and test the models. The number and nature of input parameters and the dataset size can affect the model's efficiency. The collected dataset was pre-processed to ensure that only quality data would be used in training the ML regression models. A detailed and comprehensive database consisting of 719 experimental results of rectangular CFST stub columns from 1957 to 2021 is first developed. The authors have organized the datasets very carefully. A portion of the experimental results which did not report any of the six input parameters was excluded from the database. After discarding the outliers and missing data, a total of 719 experimental datasets were considered in this study. Several previous studies used even a more extensive database which consisted of long, intermediate, and stub columns. However, the behavior of stub column and long column is completely different, and they should not be treated similarly while predicting the capacity. The statistical distributions of the design variables in the database can be seen in Fig. 2. The distributions of the specimen dimensions and the material properties in the collected

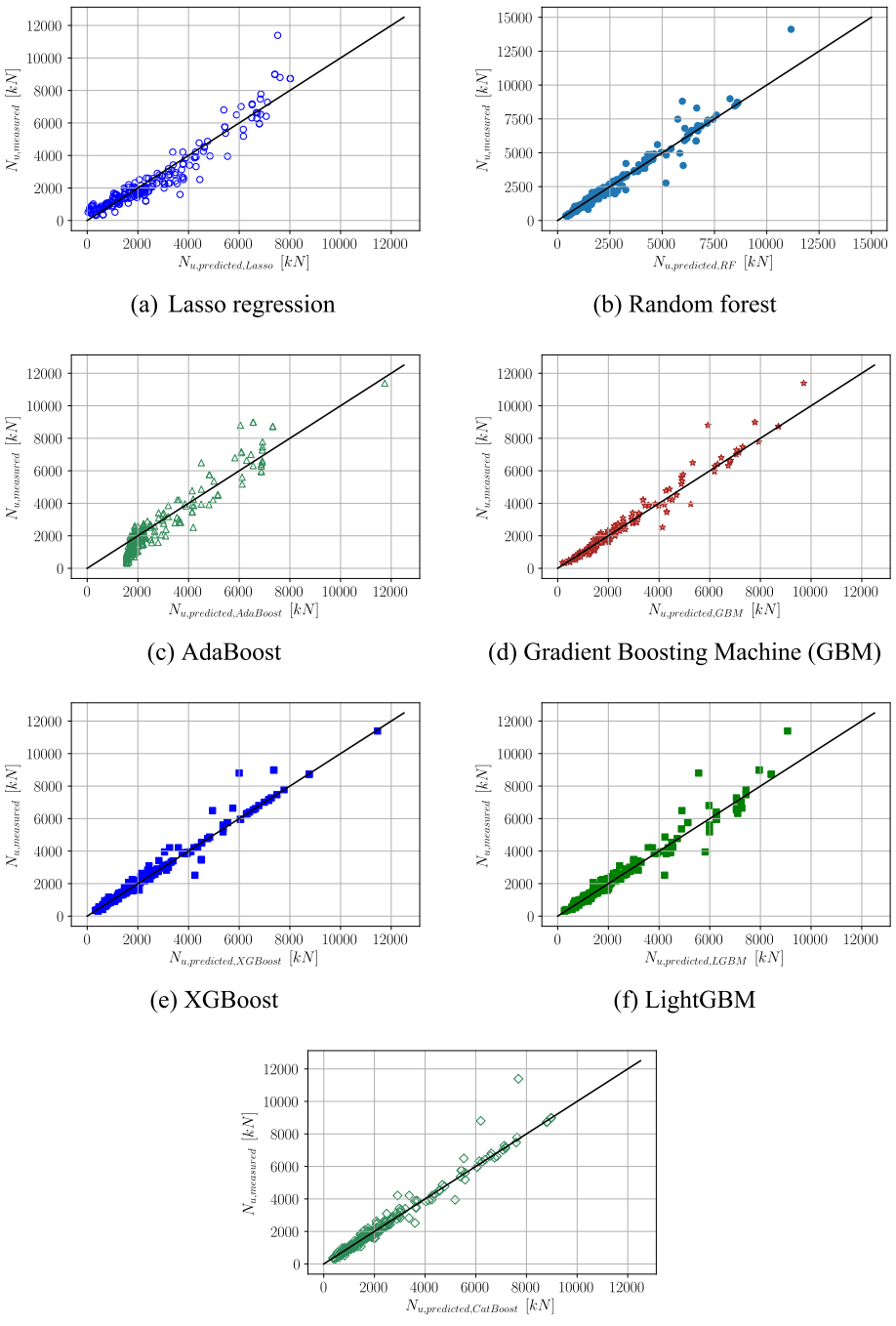

(a) Lasso regression (b) Random forest

(c) AdaBoost (d) Gradient Boosting Machine (GBM)

(e) XGBoost (f) LightGBM

(g) CatBoost

Fig. 12. Correlation between measured and predicted axial load capacities.

database are visualized in Fig. 2 using violin plots and swarm plots.

The relationships between the design variables and axial capacity are shown in Fig. 3 using a correlation matrix. It can be seen from the heat map that pairs with high correlation are demonstrated with the shades of blue, and pairs with low correlation, or inverse correlation are shown with the shades of red. Clearly, the cross-sectional side lengths and specimen heights are highly correlated with each other. The equation that computes the Pearson correlation r_{xy} between any two variables $\times$ and y is given in Eq. (11) where n is the total number of observations and x_i, y_i are the observations of the variables $\times$ and y with index i (Howell [78]).

$$r_{xy} = \frac{n\sum_{i=1}^{n} x_i y_i - \sum_{i=1}^{n} x_i \sum_{i=1}^{n} y_i}{\sqrt{n\sum_{i=1}^{n} x_i^2 - \left(\sum_{i=1}^{n} x_i\right)^2}\sqrt{n\sum_{i=1}^{n} y_i^2 - \left(\sum_{i=1}^{n} y_i\right)^2}} \tag{11}$$

4. Predictions of the ultimate compressive strength through design equations

This section presents the comparison between the measured N_u values in the experimental database and the predicted N_u values for each specimen (Figs. 4-8). Four different design standards are applied, the details of which have been elaborated in Section 2. The accuracy of each design standard has been visualized with respect to four different

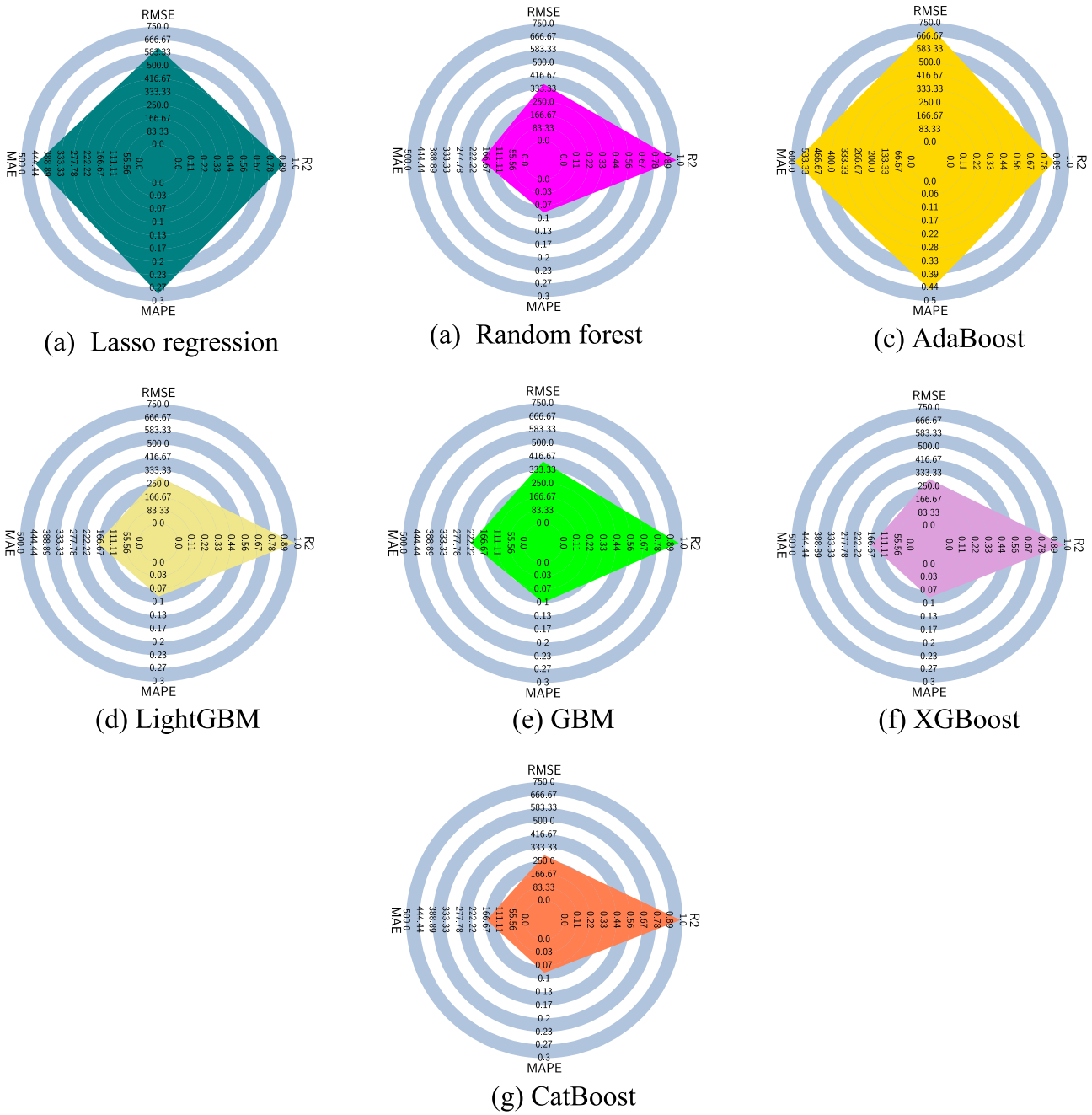

Fig. 13. Radar charts of accuracy metrics for a) Lasso regression, b) Random forest, c) AdaBoost, d)LightGBM, e) GBM, f) XGBoost, g) CatBoost.

Table 2
Performance of different code and model equations.

Design code	RMSE	R^2	MAPE	MAE
AISC 360–16	479.8	0.945	0.154	343.4
EC 4	457.6	0.950	0.116	282.2
AS-5100.6	902.0	0.806	0.278	673.8
Wang et al.[54]	424.0	0.957	0.109	266.0

accuracy metrics.

5. Proposed machine learning models

Classical ML models are “black boxes” that separate designers from mechanics. However, the recent advancement in data science has helped

Table 3
Machine learning model parameters.

Algorithm	Parameter	Range	Optimum value
CatBoost	Number of estimators	[1, 20, 100, 500, 1000]	1000
	Maximum depth of tree	[2,5,10,20]	2
	Learning rate	[0.02, 0.05, 0.1, 0.2]	0.2
LightGBM	Number of estimators	[1, 20, 100, 500, 1000]	1000
	Maximum depth of tree	[2,5,10,20]	2
	Learning rate	[0.02, 0.05, 0.1, 0.2]	0.2
XGBoost	Number of estimators	[1, 20, 100, 500, 1000]	500
	Maximum depth of tree	[2,5,10,20]	2
	Learning rate	[0.02, 0.05, 0.1, 0.2]	0.2

Table 4
Evaluation of different machine learning models.

Algorithm		RMSE	R^2	MAPE	MAE
LR	Training	616.1	0.909	0.280	439.7
	Testing	698.3	0.884	0.282	466.8
RF	Training	196.2	0.991	0.041	97.0
	Testing	372.0	0.967	0.082	186.9
AdaBoost	Training	611.6	0.911	0.394	520.6
	Testing	726.7	0.873	0.455	577.3
LightGBM	Training	135.2	0.996	0.045	81.4
	Testing	321.1	0.979	0.086	166.9
GBM	Training	201.6	0.990	0.072	143.3
	Testing	386.7	0.964	0.100	219.2
XGBoost	Training	103.8	0.996	0.043	44.1
	Testing	340.0	0.976	0.085	156.8
CatBoost	Training	122.5	0.996	0.043	71.5
	Testing	269.6	0.983	0.085	152.3

Table 5
Performance comparisons on the entire dataset.

Average value	Code equations	ML models
R^2	0.915	0.976
MAPE	0.164	0.085
MAE	391.4	165.7
RMSE	565.9	325.7

Table 6
Accuracy of the LightGBM model for different ranges of $f_c^{'}$.

$f_c^{'}$ (MPa)	R^2	MAE	MAPE	RMSE
0 – 25 (11 % of all data)	0.960	107.5	0.0697	205.2
25 – 50 (49 % of all data)	0.982	107.4	0.0614	209.5
50 – 100 (30 % of all data)	0.990	112.9	0.052	178.4
> 100 (10 % of all data)	0.995	165.8	0.0403	224.1

Table 7
Accuracy of the LightGBM model for different ranges of f_y.

f_y (MPa)	R^2	MAE	MAPE	RMSE
0 – 200 (3 % of all data)	0.963	62.5	0.0797	95.5
200 – 400 (62 % of all data)	0.974	110.6	0.0653	206.4
400 – 600 (20 % of all data)	0.994	104.3	0.0472	156.8
> 600 (15 % of all data)	0.989	158.5	0.0327	245.5

Table 8
Accuracy of the LightGBM model for different ranges of N_u.

N_u (kN)	R^2	MAE	MAPE	RMSE
0 – 2500(66 % of all data)	0.953	82.4	0.0651	120.5
2500 – 5000 (22 % of all data)	0.867	152.8	0.0466	266.3
5000 – 7500 (9 % of all data)	0.792	216.5	0.0355	321.1
> 7500 (3 % of all data)	0.913	260.3	0.0288	460.2

researchers explain the model outcomes and elucidate the complex input-output relationship to make the ML models interpretable and explainable. In the current study, seven different algorithms have been used on the database to generate predictive models. The performances of these algorithms have been compared to each other using common measures of accuracy such as the coefficient of determination (R^2). In each one of these models, the side lengths of the rectangular cross-section (*B,H*), the thickness of the steel casing (*t*), the height of the CFST specimen (*L*), the yield stress of steel (f_y) and the compressive strength of concrete (f_c') are the input variables and the ultimate axial load-carrying capacity of the columns (N_u) is the output variable. The first one of the machine learning models was generated using the Lasso regression algorithm which is a linear model that solves the minimization problem in Eq. (12) where *N* is the total number of samples, *X* is the matrix of design variable values, *w* is the vector of model coefficients, α is a constant and *y* is the vector of measurements which are compared to the model outputs.

Table 9
Accuracy of the Code Equations (AISC 360–16) for different intervals of f_y.

f_y (MPa)	R^2	MAE	MAPE	RMSE
0 – 200 (3 % of all data)	0.766	165.9	0.176	241.5
200 – 400 (62 % of all data)	0.887	314.8	0.173	433.0
400 – 600 (20 % of all data)	0.946	366.7	0.144	475.9
> 600 (15 % of all data)	0.919	467.9	0.084	671.2

Table 10
Accuracy of the Code Equations (EC4) for different intervals of $f_c^{'}$.

$f_c^{'}$ (MPa)	R^2	MAE	MAPE	RMSE
0 – 25 (11 % of all data)	0.910	177.5	0.098	307.9
25 – 50 (49 % of all data)	0.941	246.8	0.123	383.3
50 – 100 (30 % of all data)	0.930	275.2	0.108	475.6
> 100 (10 % of all data)	0.940	587.7	0.124	764.8

$$\min_{w}\left(\frac{1}{2N}\,Xw-y^2+\alpha w_1\right) \tag{12}$$

In order to achieve better performance, five more ensemble learning methods such as random forest, AdaBoost, Gradient Boosting Machine (GBM), LightGBM, XGBoost and CatBoost have been applied. Among these five models the best performance could be achieved through LightGBM, XGBoost and CatBoost algorithms with CatBoost delivering the overall best R^2 score. XGBoost being the earliest of these three algorithms, LightGBM and CatBoost were developed to improve the accuracy and convergence speed. XB (XGBoost) combines multiple base learners to enhance the model performance. The base learner is the decision tree (DT) model in this study. The major improvement in the XGBoost method over the other gradient boosting techniques is the introduction of a regularization which is achieved by modifying the loss function with an Ω term as in Eq. (13) where *T* is the number of leaves, *L* is the loss function, and w is the vector of leaf values [79,80]. The regularization parameter within the XGBoost algorithm helps overcome the generalization problem and control over-fitting, giving it better performance.

$$Obj=\sum_{i=1}^{n}L(\hat{y}_i,y_i)+\sum_{m=1}^{M}\Omega(f_k)\quad \Omega(f_k)=\gamma T+0.5\lambda||w||^2 \tag{13}$$

The LightGBM algorithm applies the gradient-based one-side sampling (GOSS) technique as opposed to the histogram-based algorithm used by XGBoost. The GOSS technique samples the data by keeping the instances with large gradients and randomly sampling the data instances with small gradients. The details of the GOSS technique can be found in Ke et al. [81]. The CatBoost algorithm uses oblivious trees due to them being less susceptible to overfitting. Another significant property of the CatBoost algorithm is the adoption of the greedy method at each new tree split. A detailed description of this algorithm can be found in Dorogush et al. [82]. Fig. 9 summarizes the entire process of predictive model development.

Table 11
Accuracy comparison of the Code Equations and ML models for different intervals of N_u.

N_u (kN)	Performance metric	Code equations	Optimum value	LightGBM
0 – 2500 (66 % of all data)	R^2	AISC 360–16	0.678	0.953
		EC4	0.814	
	MAE	AISC 360–16	243.5	82.4
		EC4	168.3	
	MAPE	AISC 360–16	0.170	0.0651
		EC4	0.121	
	RMSE	AISC 360–16	316.3	120.5
		EC4	240.4	
2500 – 5000 (22 % of all data)	R^2	AISC 360–16	0.378	0.867
		EC4	0.555	
	MAE	AISC 360–16	432.9	152.8
		EC4	327.4	
	MAPE	AISC 360–16	0.134	0.0466
		EC4	0.0998	
	RMSE	AISC 360–16	575.4	266.3
		EC4	486.9	
5000 – 7500 (9 % of all data)	R^2	AISC 360–16	−0.098	0.792
		EC4	−0.376	
	MAE	AISC 360–16	624.5	216.5
		EC4	683.6	
	MAPE	AISC 360–16	0.098	0.0355
		EC4	0.107	
	RMSE	AISC 360–16	738.6	321.1
		EC4	826.9	
>7500 (3 % of all data)	R^2	AISC 360–16	0.416	0.913
		EC4	0.206	
	MAE	AISC 360–16	1064.1	260.3
		EC4	1278.7	
	MAPE	AISC 360–16	0.118	0.0288
		EC4	0.137	
	RMSE	AISC 360–16	1195.6	460.2
		EC4	1393.7	

5.1. Machine learning model performance measures

The performance of the proposed seven ML models is compared using different statistical measures. Root mean square error (RMSE), coefficient of determination (R^2), mean absolute error (MAE), and mean absolute percentage error (MAPE) were found to be the most commonly used performance metrics in the literature and are also used in this study. The equations of the four statistical measures are given below:

$$RMSE = \sqrt{\frac{\sum_{i=1}^{n}(y_i - \widetilde{y}_i)^2}{n}} \tag{14}$$

$$R^2 = \left(\frac{n\sum_{i=1}^{n} y_i \widetilde{y}_i - \sum_{i=1}^{n} y_i \sum_{i=1}^{n} \widetilde{y}_i}{\sqrt{n\sum_{i=1}^{n} y_i^2 - \left(\sum_{i=1}^{n} y_i\right)^2} \sqrt{n\sum_{i=1}^{n} \widetilde{y}_i^2 - \left(\sum_{i=1}^{n} \widetilde{y}_i\right)^2}} \right)^2 \tag{15}$$

$$MAPE = \frac{1}{n}\sum_{i=1}^{n} \frac{\left|y_i - \widetilde{y}_i\right|}{max\left(\epsilon, \left|y_i\right|\right)} \tag{16}$$

$$MAE = \frac{\sum_{i=1}^{n}\left|y_i - \widetilde{y}_i\right|}{n} \tag{17}$$

RMSE, MAE, and MAPE values close to zero are indicators of good model performance. The values of R^2 represent the fitness of the predictive model such that R^2 values close to 1 indicate ideal model fitness.

In the following section, the N_u values predicted by the design codes AISC 360–16 [45], EC 4 [46] and AS 5100 [47] were compared against the actual experimental measurements. The root mean square error (RMSE), coefficient of determination (R^2), mean absolute percentage error (MAPE) and mean absolute error (MAE) values of these design code equations were calculated using Eqs. (14) to (17) where y_i and $\widetilde{y}_i$ stand for the measured and predicted values, respectively. In Eq. (16), ϵ stands for a relatively small positive number that serves the purpose of preventing division by zero.

It should be noted that the experimental database includes measurements where the yield stress of the steel casing is above the maximum yield stress for which the AISC 360–16 equation is deemed applicable, which is 525 MPa. Also, according to AISC 360–16 the concrete compressive strength should not be >70 MPa, whereas the experimental database includes f_c' values above this upper bound. The RMSE, R^2, MAPE and MAE values corresponding to various design code equations are listed in Table 1. In Table 1 also the upper bounds for f_y and f_c' are given below which the equations are applicable.

5.2. Hyperparameter tuning and cross-validation

Among the machine learning models, XGBoost, CatBoost, and LightGBM were found to perform better than the remaining algorithms. For these three algorithms, the number of trees (n_estimators), learning rate and the maximum tree depth are optimized as the most significant parameters, whose value grids are respectively defined as [1, 20, 100, 500, 1000], [0.02, 0.05, 0.1, 0.2], and [2,5,10,20]. A list of the parameter values that delivered the best results is given in Table 3. Furthermore, for the XGBoost algorithm, the model performance has been visualized as a function of the number of trees and the learning rate in Fig. 10. As Fig. 10 shows, the selection of the learning rate as 0.2 delivered the best performance for all tree numbers.

As a first attempt to generate a model that predicts N_u, the database has been randomly divided into training and testing sets. Past literature revealed that training–testing divisions have relatively less impact on the final model performance. For instance, Feng et al. [59] and Nguyen et al. [85], and many other studies used 70 % of the dataset for training and 30 % of the dataset for testing. All those studies reported high model performance utilizing 70/30 train/test ratio. Based on the past studies and relative model performance (Hastie et al. [86]), authors have adopted the most common dataset division which is 70 % to 30 % train/test ratio in the current study. The 70 % training datasets are used for hyperparameters tuning using the grid search method. A summary of the hyperparameters generated for the proposed ML models is presented in Table 3. After the 70 % to 30 % split of the database into a training and a test set, a 10-fold cross-validation was applied to the training set. The 10-fold cross-validation procedure divides the training set into 10 disjoint groups. Each of these groups serves as a test set once while the remaining 9 groups are used to fit the model. Later the trained model is

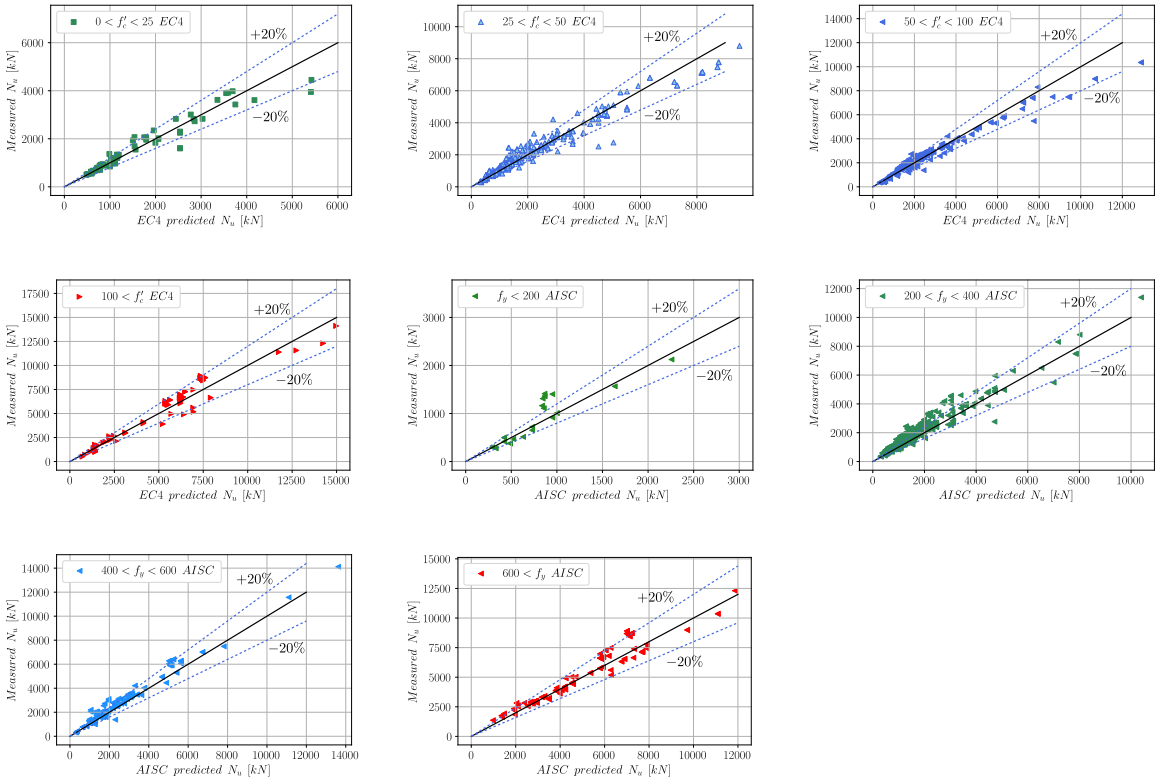

Fig. 14. Predictions of EC4 and AISC 360–16 on different intervals of f_c' and f_y.

evaluated using this test set. The mean performance of the 10 different models is reported at the end. This technique estimates the model's expected performance on new data that has not been used in training the model. This procedure is illustrated in Fig. 11. A "random state" was assigned for each ML model using Python scikit-learn package so that both the training and test database contain identical specimens.

5.3. Predictions of the machine learning algorithms

This section presents the predictions of seven different machine learning models on the training and test sets. For each model, the optimum parameter values from Table 3 have been used. As the input variables of the models the side lengths of the rectangular cross-section (*B,H*), the thickness of the steel casing (t), the height of the CFST specimen (*L*), the yield stress of steel (f_y) and the compressive strength of concrete (f_c') were selected. The elasticity moduli of steel and concrete were omitted since these variables do not exhibit a wide variance. For each machine learning model, the comparison of the measured and predicted N_u values have been plotted in Fig. 12 for the entire dataset. Furthermore, the accuracy values of the predictions have been visualized in Fig. 13 with the help of radar charts using four different metrics of accuracy. In Fig. 13 all accuracy metrics are representative of the performance of the corresponding model on the test set.

A comparison of the model performances in Table 4 with the code equation performances in Table 2 shows that the Random Forest, LightGBM, XGBoost and CatBoost models performed better than all code equations in terms of R^2 score with an average R^2 value of 0.976. Compared to the average R^2 value of 0.915 of the code equations this corresponds to a 6.7 % improvement. Furthermore, the best performing four ML models are observed to have an average MAPE value of 0.085, an average MAE of 165.7 and an average RMSE value of 325.7. In comparison, the code equations have MAPE, MAE, and RMSE values of 0.164, 391.4 and 565.9, respectively. It should be noted that the performances in Table 5 were measured based on the entire database. In order to better understand whether the equations and the ML models perform equally good on different variable ranges, the input variables f_y, f_c' in addition to the output variable N_u have been split into different intervals and the code equations and the ML models have been separately tested on these different intervals. Table 6, Table 7 and Table 8 show the performance of the LightGBM algorithm for different ranges of f_c', f_y and N_u respectively.

It can be observed that for data samples with high strength such as $50< f_c$' and $400< f_y$ the LightGBM algorithm performed particularly well. Also, the algorithm demonstrated above average performance, compared to the average values in Table 5, in all material property ranges and for all metrics except for the R^2 score for the range of $0< f_y <400$ and $0< f_c$' <25. On the other hand, the algorithm had a slightly below average R^2 score for $0< f_c$' <25 which corresponds to 11 % of the entire database and for $0< f_y <200$ which makes up 3 % of all data samples. In addition to the material properties also, the performance of the LightGBM algorithm has been investigated at different intervals of N_u. Since the top four ML algorithms have similar performances, only one of them (LightGBM) has been used in order to present the ML algorithm performance. It was observed that at certain intervals of N_u the ML predictions are not as good as the predictions on the entire dataset. In order to compare this performance to the code equations the performance of the AISC 360–16 and EC4 equations have been listed in Tables 9-11.

Table 9 and Table 10 show that the MAE and RMSE values of the code equations are increasing with material strength. A similar tendency could also be observed for the MAE and RMSE values of the LightGBM algorithm with the exception of the interval $400< f_y <600$ in which the RMSE value of the LightGBM algorithm was smaller than the previous interval with the lower material strength. However, in every interval of the material strengths the LightGBM algorithm is observed to have significantly lower MAE and RMSE values. In addition to that for 200<

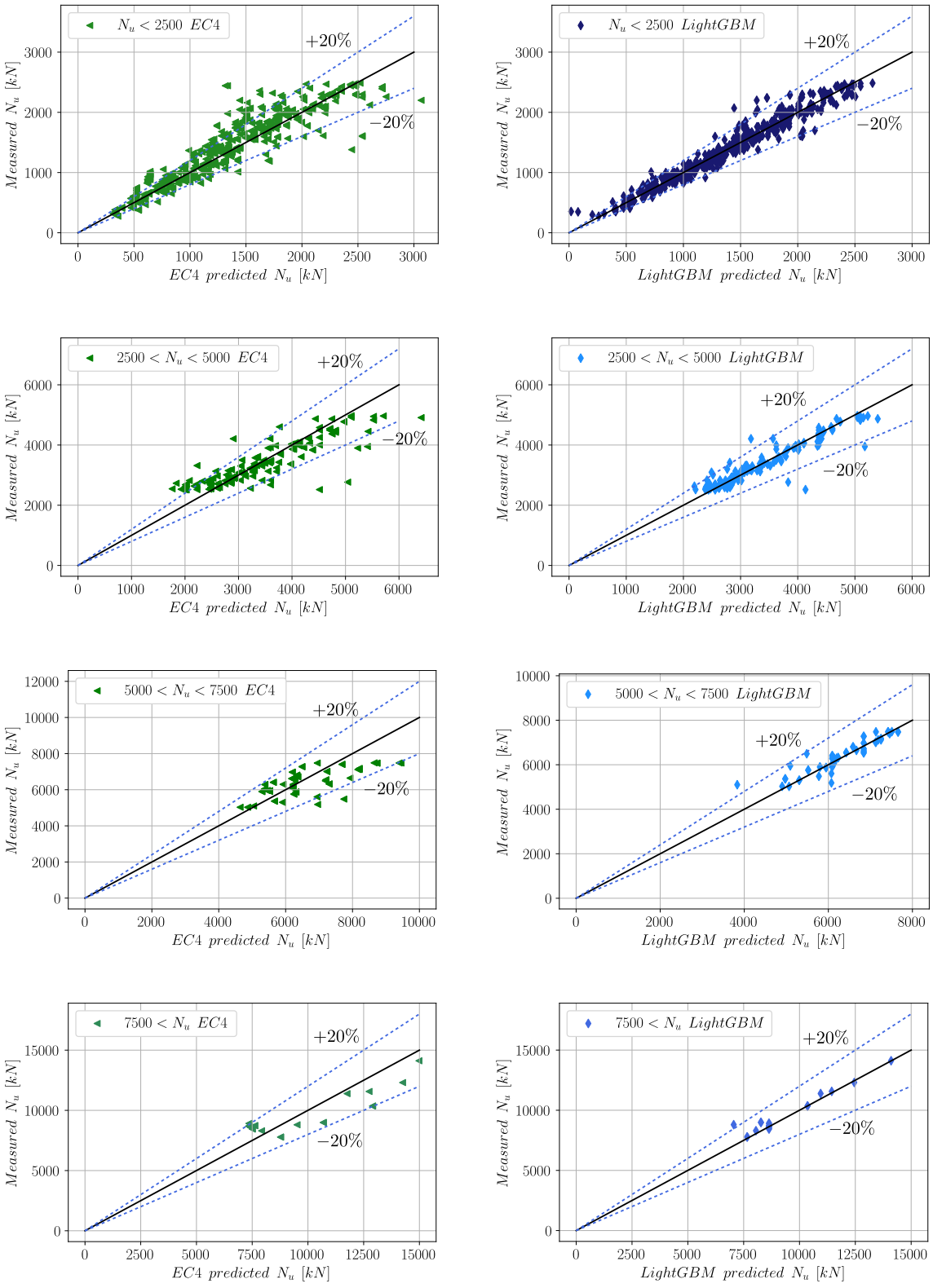

Fig. 15. Comparison of code equations and LightGBM on different intervals of N_u.

f_y <400 which makes up 62 % of all samples, the AISC 360–16 equations have an R^2 value of 0.887 which is significantly lower than the R^2 value obtained through the LightGBM algorithm. Also, for all intervals of f_y and f_c' the MAPE values obtained through the LightGBM algorithm were at least 41 % lower than the MAPE values corresponding to the code equations. For $f_c' > 100$ the MAPE value associated with the EC4 equation was 208 % greater than the MAPE value of the LightGBM algorithm. Greater performance differences between the code equations

Table 12
ML model validation data points (Yu et al. [44]).

ID	B (mm)	H (mm)	t (mm)	L (mm)	f_y(MPa)	$f_c^{'}$(MPa)	N Test (kN)
R1-1	120	120	4	360	495	60	1701
R1-2	120	120	4	360	495	60	1657
R4-1	130	130	4	390	495	60	2020
R4-2	130	130	4	390	495	60	2018
R7-1	106	106	4	320	495	89	1749
R7-2	106	106	4	320	495	89	1824
R10-1	140	140	4	420	495	89	2752
R10-2	140	140	4	420	495	89	2828
A1	120	120	5.8	360	300	83	1697
A2	120	120	5.8	360	300	106	1919
A3-1	200	200	5.8	600	300	83	3996
A3-2	200	200	5.8	600	300	83	3862
A9-1	120	120	4	360	495	55	1739
A9-2	120	120	4	360	495	55	1718
A12-1	130	130	4	390	495	55	1963
A12-2	130	130	4	390	495	55	1988
S1	127	127	3.2	611	356	30.5	917
S2	127	127	4.3	608	357	26	1095
S3	127	127	4.6	609	322	23.8	1113
S4	127	127	5.7	607	312	23.8	1202
S5	127	127	7.5	610	347	23.8	2069

Table 13
Performance of different ML models validation using additional test data from Table 12.

Algorithm	RMSE	R^2	MAPE	MAE
XGBoost	93.4	0.986	0.043	74.5
LightGBM	198.1	0.935	0.072	141.3
Random Forest	148.9	0.963	0.034	80.7
CatBoost	193.1	0.938	0.078	157.4

Table 14
Performance of different code and model equations using additional test data from Table 12.

Design code	RMSE	R^2	MAPE	MAE
AISC 360–16	243.4	0.902	0.100	198.0
EC 4	194.4	0.937	0.069	146.7
AS-5100.6	556.7	0.486	0.278	524.3
Wang et al.[54]	172.4	0.951	0.065	136.0

and the ML models could be observed at certain intervals of N_u as can be seen in Table 11. From Table 11, it is clear that the code equation performance was not satisfactory for certain intervals of N_u. Particularly for 5000kN < N_u <7500kN the R^2 score of both code equations was negative, which indicates poor performance. In all intervals of N_u the LightGBM algorithm performed significantly better for all performance metrics. The performances of the code equations and the LightGBM model on different variable intervals are shown in Fig. 14 and Fig. 15.

5.4. Machine learning model validation with additional data

In order to have further validation of the machine learning models against independent data outside the data pool, further data points have been collected from the literature. 21 additional data points from Yu et al. [44] (Table 12) have been utilized to test the performance of the machine learning models. The performances of the ML models and the prediction equations on the newly added data points are presented in Table 13 and Table 14, respectively. It can be observed that the XGBoost model outperformed all of the equation predictions as well as the other

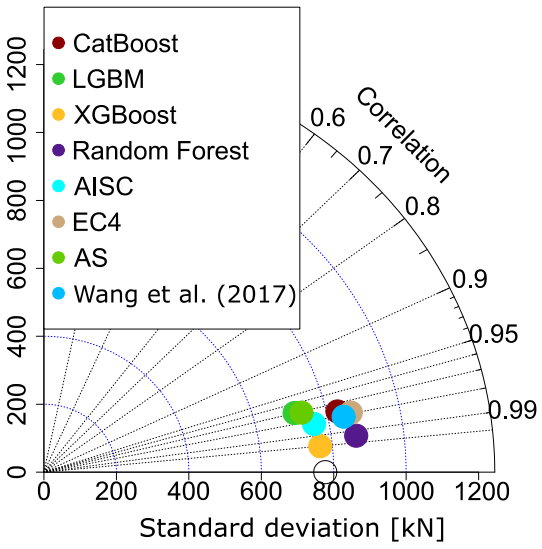

Fig. 16. Taylor diagram showing ML models and various code performances in predicting the compressive capacity of CFST columns.

ML models. Furthermore, the Random Forest (RF) model is also observed to perform better than the equations. Among the prediction equations the equation of Wang et al. performed better than the other equations, whereas the AS-5100.6 equation performed worst. The performances of the ML models and the equations are also visualized with a Taylor diagram in Fig. 16 where the standard deviations of the test data and the predicted values are shown on the horizontal and vertical axes. The radial grid in Fig. 16 shows the Pearson correlation coefficient between the predicted values and the actual test data. It can be observed that the XGBoost model is also the highest performer in terms of the Pearson correlation.

6. Feature importance analyses

The relative feature importance values in Fig. 17 indicate the impact of different input variables on the predicted compressive strength. The sum of the feature importance values of each input variable in Fig. 17 adds up to 100 for each algorithm. The feature importance analysis of the two best-performing algorithms showed that the yield strength of steel casing and the compressive strength of the concrete infill have greater importance in terms of their effect on the structural performance in the LightGBM models. On the other hand, cross-sectional side length B appeared to have greater importance than f_c' in the CatBoost model. In both models, the column length L was observed to have the least impact on the model output.

7. Interpretation of the ML models

The effect of different geometric and material parameters on the final prediction has been quantified using the SHAP technique. This technique assigns a SHAP value to each design parameter as shown in Fig. 18. The SHAP model can be summarized as in Eq. (18) where M is the number of design variables, ϕ_i are the SHAP values corresponding to i-th design variable and x' is a simplified vector of design variables that is related to the actual design values through a mapping function. A detailed explanation about SHAP can be found in Mangalathu et al. [57] and Feng et al. [60].

$$s(x^{'}) = \phi_0 + \sum_{i=1}^{M} \phi_i x_i^{'} \tag{18}$$

Fig. 18 shows the distribution of the SHAP values based on the XGBoost model. In Fig. 18 positive SHAP values indicate that the

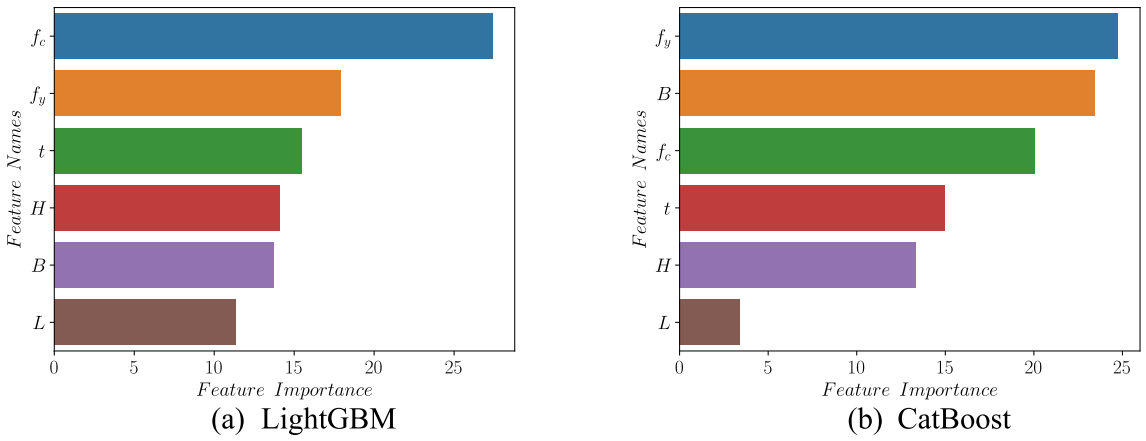

Fig. 17. The feature importance analyses using a) LightGBM and b) CatBoost algorithms.

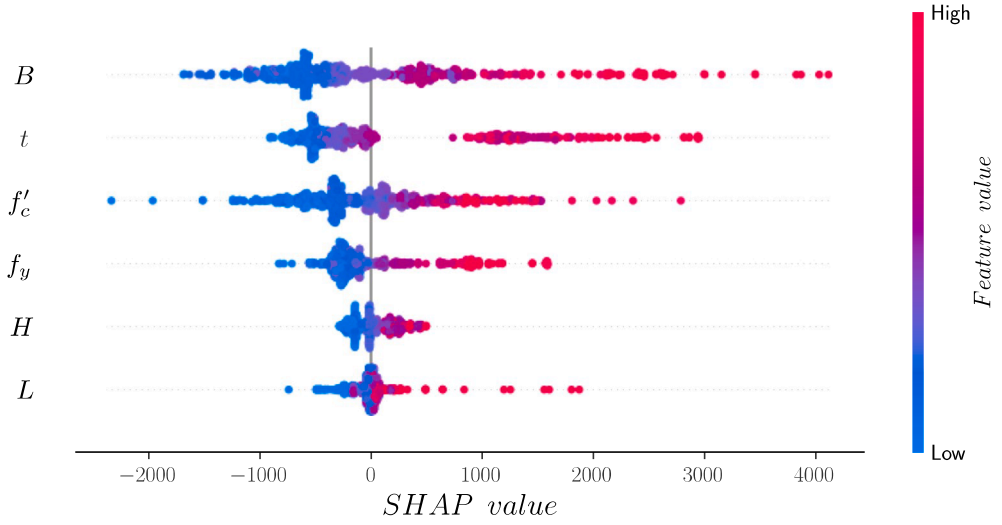

Fig. 18. Model interpretation through SHAP summary plot.

variable has a positive effect on N_u and a negative value indicates a negative effect of the corresponding variable. The impact of a variable on N_u is proportional to the magnitude of its SHAP value. The design variables are ordered along the vertical axis with respect to their impact on the output. It follows that the side length b, the wall thickness t and the compressive strength of concrete have the greatest effect on N_u.

The feature dependencies shown in Fig. 19 supplement Fig. 18 by giving further information about the change of the SHAP value with respect to design variable values. The feature dependence plots in Fig. 19 contain information about the effect of a feature on the predicted outcome. For each feature in Fig. 19 the design variable most dependent on that feature is shown with a colored bar on the right side of the plot. Fig. 19 shows that the SHAP value increases with increasing values of all design variables. Therefore, N_u is positively correlated with all design variables. Also, Fig. 19c shows that for t values>6 mm the SHAP value changes its sign, and there is a rapid increase in N_u. Similarly, for $b >$ 150 mm, $h >$ 150 mm, $l >$ 1000 mm, $f_y >$ 500 MPa and $f_c' >$ 50 MPa a rapid increase in N_u can be observed. Fig. 19 also contains information about the variation of the SHAP value according to multiple design variables. As an example, Fig. 19c shows that for $t <$ 6 mm, lower values of b correspond to higher SHAP values, whereas for $t >$ 6 mm greater b values lead to greater SHAP values. The developed Python-based interactive notebook and ensembled ML models used to predict the capacity of CFST columns can be found at https://www.kaggle.com/code/celalakrolu/cfst-ml.

8. Resistance factor

In load and resistance factor design, the resistance factor (ϕ) takes the uncertainties in the design process into account. Using the predictions obtained through ML algorithms and the experimental database, the resistance factor is calculated using Eq. (19), where P is the mean value of the measured to predicted compressive strength ratio. The P value was calculated as 1.0 by taking the mean value of the ratio of the N_u measurements available in the database and the N_u values predicted by the CatBoost model ($N_{u,measured}/N_{u,predicted}$).

$$\phi = (P{\cdot}M{\cdot}F)e^{(-\alpha\beta V_R)} \tag{19}$$

In Eq. (19), V_R is the coefficient of resistance which is a function of the variables V_M, V_F and V_P. The coefficient of resistance is defined as $V_R = \sqrt{{V_M}^2 + {V_F}^2 + {V_P}^2}$ where V_P is the coefficient of variation of the $N_{u,measured}/N_{u,predicted}$ ratio. The variables V_M and V_F stand for the coefficient of variation for material and fabrications, respectively. The V_P value was calculated as 0.09. The V_F and V_M values are taken as 0.05 and 0.193 based on Ravindra and Galambos [87] and Sener and Varma [88], respectively. The reliability index β and the linearization approximation constant α are assigned the values of 3.0 and 0.7 based on Ravindra and Galambos [87] and ASCE 2017 [89], respectively. The value of the mean ratio of measured-to-nominal cross-sectional properties F is conservatively assigned the value of 1.0. The mean ratio of the measured-to-nominal material strengths M is assigned the value of 1.19 according

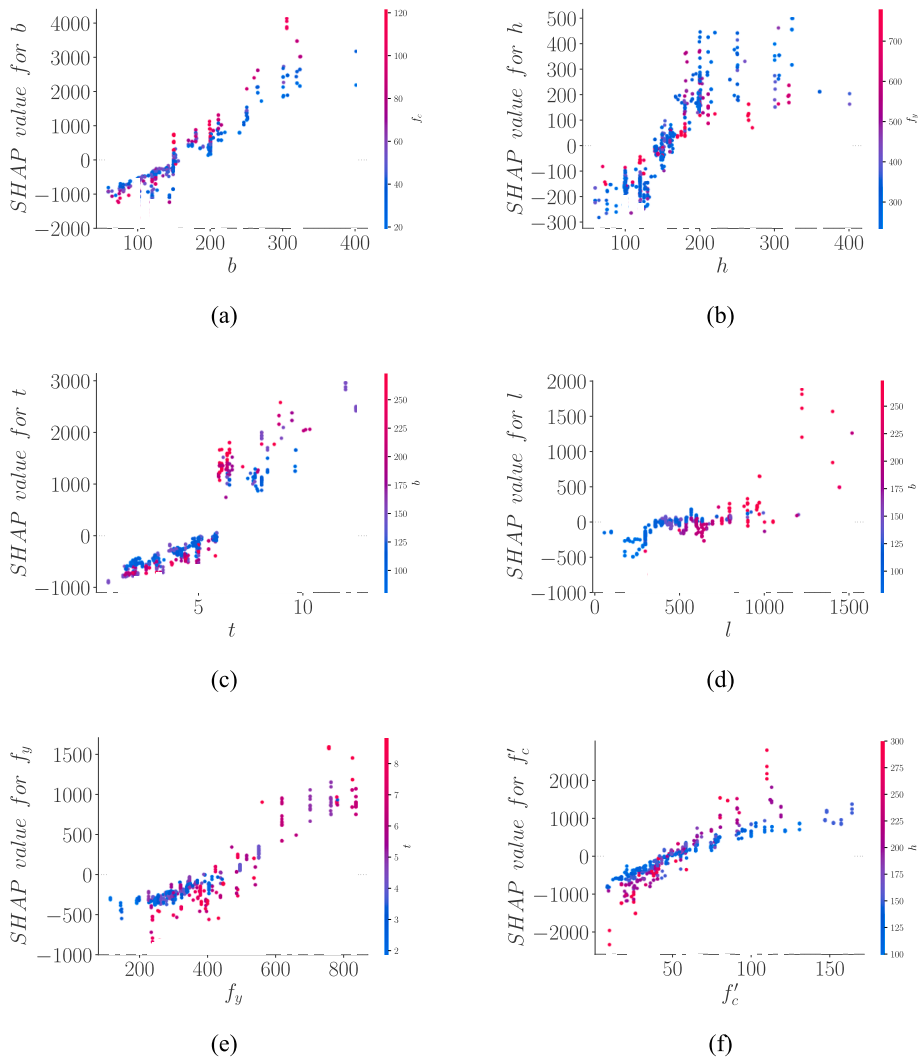

Fig. 19. Feature dependence plots: a) b, b) h, c) t, d) l, e) f_y, f) f_c'.

to material properties in the experimental database and Thai et al. [90]. Plugging these values in Equation (19) yields the resistance factor of 0.75, which is equal to the AISC 360–16 [45] recommended resistance factor.

9. Summary and conclusions

The current study developed ensemble ML models to predict the ultimate axial compressive capacity of rectangular CFST stub columns under compression. A comprehensive database of CFST stub columns is utilized to develop the explainable ML models, including lasso regression, random forest, AdaBoost, GBM, LightGBM, XGBoost, and CatBoost. Six input parameters are considered, such as the width and depth of column cross-section, the thickness of steel tube, the height of the column, the yield strength of steel, and the concrete compressive strength for predicting cross-sectional resistance of CFST column. Hyperparameter tuning and 10-fold cross-validations are performed to develop the ML model. SHapley Additive exPlanations is used to explain the input-output relationship of the best-performing model. The following conclusions can be drawn based on the present study:

- The trained ensemble learning models were able to make predictions of the ultimate compressive strength of rectangular stub columns with better accuracy than the available code equations.
- The best performing ML model is CatBoost, with a coefficient of determination equal to 98.3 %. LightGBM model is found to be the second-best performing model.
- The improvement in the prediction accuracy was particularly pronounced for certain intervals of N_u, f_y and f_c'. The code equations demonstrated poor performance for N_u values >7500kN, whereas the LightGBM algorithm reached an R^2 value of 91.3 % for specimens in this range.
- For f_y <400 MPa, which corresponds to 65 % of the entire database, the ensemble learning models significantly outperformed the code equations. An increase in f_c' and f_y was associated with increased MAE for both code equations, whereas for the LightGBM algorithm, an apparent increase in MAE was only observed for f_c' >100 MPa and f_y >600 MPa. For all ranges of material properties and N_u the MAE value of the LightGBM algorithm was significantly smaller than the code equations.
- The feature importance analyses reveal that the most important features are the strength of materials used in predicting the cross-sectional resistance of CFST columns.
- The SHAP model for interpreting the ensemble learning models indicates that the side length b of the cross-section has the highest impact on the predicted compressive load capacity followed by t, f_c', f_y, h and l. Feature dependence plots showed that the SHAP value increases with increasing values of all design variables.

- The resistance factor is determined using AISC 360–16 provision and is found to be 0.75 through the CatBoost model.
- The proposed explainable ML models can easily be extended to other composite columns, beams, and frames capacity prediction.

Future research in this field can include the effect of eccentric loading on the axial load carrying capacity. Furthermore, columns with high slenderness can be included in the study in addition to stub columns. Using FE analysis to predict the compressive strength, new data points can be obtained for configurations for which no experimental data is available. Using this combined approach, the limitation on the number of available data samples can be largely overcome.

The authors believe that mechanics-based and semi-empirical models should be utilized in parallel with the data-driven ML models to design or perform the existing structure's performance evaluation/retrofitting. ML models are robust, dynamic, reliable, and fast, but they should not replace the traditional approaches; instead, both approaches should augment each other to help practicing engineers during the design and evaluation process and help research scientists plan a more comprehensive experimental program.

CRediT authorship contribution statement

Celal Cakiroglu: Methodology, Visualization, Formal analysis, Writing – original draft. **Kamrul Islam:** Conceptualization, Data curation, Writing – original draft. **Gebrail Bekdaş:** Methodology, Supervision. **Umit Isikdag:** Software, Supervision. **Sujith Mangalathu:** Conceptualization, Writing – review & editing.

Declaration of Competing Interest

The authors declare that they have no known competing financial interests or personal relationships that could have appeared to influence the work reported in this paper.

Data availability

Data will be made available on request.

References

[1] B. Uy, Strength of short concrete filled high strength steel box columns, Journal of Constructional Steel Research 57 (2) (2001) 113–134.
[2] A.H. Varma, J.M. Ricles, R. Sause, L.W. Lu, Seismic behavior and modeling of high-strength composite concrete-filled steel tube (CFT) beam–columns, Journal of Constructional Steel Research 58 (5–8) (2002) 725–758.
[3] A.H. Varma, J.M. Ricles, R. Sause, L.W. Lu, Experimental behavior of high strength square concrete-filled steel tube beam-columns, Journal of Structural Engineering 128 (3) (2002) 309–318.
[4] K. Sakino, H. Nakahara, S. Morino, I. Nishiyama, Behavior of centrally loaded concrete-filled steel-tube short columns, Journal of structural engineering 130 (2) (2004) 180–188.
[5] D. Liu, W.M. Gho, Axial load behaviour of high-strength rectangular concrete-filled steel tubular stub columns, Thin-Walled Structures 43 (8) (2005) 1131–1142.
[6] Zhong, S. T. (2006). Unified theory of CFST: research and application.
[7] G.D. Hatzigeorgiou, Numerical model for the behavior and capacity of circular CFT columns, Part I: Theory. Engineering Structures 30 (6) (2008) 1573–1578.
[8] G.D. Hatzigeorgiou, Numerical model for the behavior and capacity of circular CFT columns, Part II: Verification and extension, Engineering Structures 30 (6) (2008) 1579–1589.
[9] P.R. Munoz, C.T.T. Hsu, Behavior of biaxially loaded concrete-encased composite columns, Journal of Structural Engineering 123 (9) (1997) 1163–1171.
[10] L.H. Han, W. Li, R. Bjorhovde, Developments and advanced applications of concrete-filled steel tubular (CFST) structures: Members, Journal of constructional steel research 100 (2014) 211–228.
[11] Shieh, S. S., Chang, C. C., & Jong, J. H. (2003, October). Structural design of composite super-columns for the Taipei 101 Tower. In Proceedings of International Workshop on Steel and Concrete Composite Constructions (pp. 25-33).
[12] W. Huang, Z. Lai, B. Chen, Z. Xie, A.H. Varma, Concrete-filled steel tube (CFT) truss girders: Experimental tests, analysis, and design, Engineering Structures 156 (2018) 118–129.
[13] Lai, Z., Huang, Z., & Varma, A. H. (2017, February). Seismic analysis and performance of high strength composite special moment frames (C-SMFs). In Structures (Vol. 9, pp. 165-178). Elsevier.
[14] B. Chen, Z. Lai, Q. Yan, A.H. Varma, X. Yu, Experimental behavior and design of CFT-RC short columns subjected to concentric axial loading, Journal of Structural Engineering 143 (11) (2017) 04017148.
[15] K. Klöppel, W. Goder, Traglastversuche mit ausbetonierten Stahlrohen und Aufstellung einer Bemessungsformel, Der Stahlbau 26 (1) (1957) 1–10.
[16] Q.X. Ren, K. Zhou, C. Hou, Z. Tao, L.H. Han, Dune sand concrete-filled steel tubular (CFST) stub columns under axial compression: experiments, Thin-walled structures 124 (2018) 291–302.
[17] L.H. Han, Tests on stub columns of concrete-filled RHS sections, Journal of Constructional Steel Research 58 (3) (2002) 353–372.
[18] M. Shams, M.A. Saadeghvaziri, State of the art of concrete-filled steel tubular columns, Structural Journal 94 (5) (1997) 558–571.
[19] S.P. Schneider, Axially loaded concrete-filled steel tubes, Journal of structural Engineering 124 (10) (1998) 1125–1138.
[20] L.H. Han, G.H. Yao, X.L. Zhao, Tests and calculations for hollow structural steel (HSS) stub columns filled with self-consolidating concrete (SCC), Journal of Constructional Steel Research 61 (9) (2005) 1241–1269.
[21] L.H. Han, G.H. Yao, Z. Tao, Performance of concrete-filled thin-walled steel tubes under pure torsion, Thin-Walled Structures 45 (1) (2007) 24–36.
[22] L.H. Han, Z.B. Wang, W. Xu, Z. Tao, Behavior of concrete-encased CFST members under axial tension, Journal of Structural Engineering 142 (2) (2016) 04015149.
[23] R.B. Ali, M. Islam, M. Begum, M. Rahman, Behavior of concrete-filled steel tubular cold-formed built-up slender square columns under eccentric compression, Innovative Infrastructure Solutions 6 (4) (2021) 1–18.
[24] T.T.J.G. Yu, J.G. Teng, Y.L. Wong, S.L. Dong, Finite element modeling of confined concrete-I: Drucker-Prager type plasticity model, Engineering structures 32 (3) (2010) 665–679.
[25] K. Sakino, Sustaing Load Capacity of Plain Concrete Stub Columns Confined by Circular Steel Tube, in: In ProceedIngs of the International Speciality Conference on Concrete Filled Steel Tubular Structures, 1985, pp. 112–118.
[26] F. Huang, X. Yu, B. Chen, The structural performance of axially loaded CFST columns under various loading conditions, Steel & Composite Structures 13 (5) (2012) 451–471.
[27] J. Liu, X. Zhou, S. Zhang, Seismic behaviour of square CFT beam–columns under biaxial bending moment, Journal of Constructional Steel Research 64 (12) (2008) 1473–1482.
[28] G.W. Zhang, Y. Xiao, S. Kunnath, Low-cycle fatigue damage of circular concrete-filled-tube columns, ACI Structural Journal 106 (2) (2009) 151.
[29] T. Perea, R.T. Leon, J.F. Hajjar, M.D. Denavit, Full-scale tests of slender concrete-filled tubes: Interaction behavior, Journal of Structural Engineering 140 (9) (2014) 04014054.
[30] A.Y. Jiang, J. Chen, W.L. Jin, Experimental investigation and design of thin-walled concrete-filled steel tubes subject to bending, Thin-Walled Structures 63 (2013) 44–50.
[31] Y.F. Yang, G.L. Ma, Experimental behaviour of recycled aggregate concrete filled stainless steel tube stub columns and beams, Thin-Walled Structures 66 (2013) 62–75.
[32] Y. Ye, L.H. Han, Z. Tao, S.L. Guo, Experimental behaviour of concrete-filled steel tubular members under lateral shear loads, Journal of Constructional Steel Research 122 (2016) 226–237.
[33] Z.B. Wang, L.H. Han, W. Li, Z. Tao, Seismic performance of concrete-encased CFST piers: experimental study, Journal of Bridge Engineering 21 (4) (2016) 04015072.
[34] Z. Tao, U.Y. Brian, L.H. Han, S.H. He, Design of concrete-filled steel tubular members according to the Australian Standard AS 5100 model and calibration, Australian Journal of Structural Engineering 8 (3) (2008) 197–214.
[35] Z. Tao, U. Katwal, B. Uy, W.D. Wang, Simplified Nonlinear Simulation of Rectangular Concrete-Filled Steel Tubular Columns, Journal of Structural Engineering 147 (6) (2021) 04021061.
[36] R.T. Leon, T. Perea, J.F. Hajjar, M.D. Denavit, Concrete-filled tubes columns and beam-columns: a database for the AISC 2005 and 2010 specifications, Festschrift Gerhard Hanswille 20 (2011) 203–212.
[37] Hajjar, J. F., Gourley, B. C., Tort, C., Denavit, M. D., Schiller, P. H., & Mundis, N. L. (2013). Steel-concrete composite structural systems. Department of Civil and Environmental Engineering, Northeastern University.
[38] Z. Lai, A.H. Varma, K. Zhang, Noncompact and slender rectangular CFT members: Experimental database, analysis, and design, Journal of Constructional Steel Research 101 (2014) 455–468.
[39] Z. Lai, E.C. Fischer, A.H. Varma, Database and review of beam-to-column connections for seismic design of composite special moment frames, Journal of Structural Engineering 145 (5) (2019) 04019023.
[40] Z. Lai, A.H. Varma, Noncompact and slender circular CFT members: Experimental database, analysis, and design, Journal of Constructional Steel Research 106 (2015) 220–233.
[41] Z. Lai, A.H. Varma, High-strength rectangular CFT members: Database, modeling, and design of short columns, Journal of Structural Engineering 144 (5) (2018) 04018036.
[42] S. Thai, H.T. Thai, B. Uy, T. Ngo, Concrete-filled steel tubular columns: Test database, design and calibration, Journal of Constructional Steel Research 157 (2019) 161–181.
[43] M. Yu, X. Zha, J. Ye, C. She, A unified formulation for hollow and solid concrete -filled steel tube columns under axial compression, Engineering Structures 32 (4) (2010) 1046–1053.

[44] M. Yu, X. Zha, J. Ye, Y. Li, A unified formulation for circle and polygon concrete-filled steel tube columns under axial compression, Engineering Structures 49 (2013) 1–10.
[45] AISC. (2016). "Specification for structural steel buildings." AISC 360-16, Chicago.
[46] EN 1994-1-1. Eurocode 4: Design of composite steel and concrete structures – Part 1-1: General rules and rules for buildings, European Committee for Standardization; 2004.
[47] AS-5100.6, Australian Standard. Part 6: Steel and composite construction, (2004).
[48] Y. Du, Z. Chen, J.R. Liew, M.X. Xiong, Rectangular concrete-filled steel tubular beam-columns using high-strength steel: Experiments and design, Journal of constructional steel research 131 (2017) 1–18.
[49] B. Uy, Stability and ductility of high performance steel sections with concrete infill, Journal of Constructional Steel Research 64 (7–8) (2008) 748–754.
[50] F. Aslani, B. Uy, Z. Tao, F. Mashiri, Behaviour and design of composite columns incorporating compact high-strength steel plates, Journal of Constructional Steel Research 107 (2015) 94–110.
[51] Uy, B., Khan, M., Tao, Z., & Mashiri, F. (2013). Behaviour and design of high strength steel-concrete filled columns. In Proceedings of the 2013 world congress on advances in structural engineering and mechanics (ASEM13), Jeju, Korea (pp. 150-167).
[52] H.T. Thai, B. Uy, M. Khan, Z. Tao, F. Mashiri, Numerical modelling of concrete-filled steel box columns incorporating high strength materials, Journal of Constructional Steel Research 102 (2014) 256–265.
[53] M. Khan, B. Uy, Z. Tao, F. Mashiri, Behaviour and design of short high-strength steel welded box and concrete-filled tube (CFT) sections, Engineering Structures 147 (2017) 458–472.
[54] Z.B. Wang, Z. Tao, L.H. Han, B. Uy, D. Lam, W.H. Kang, Strength, stiffness and ductility of concrete-filled steel columns under axial compression, Engineering Structures 135 (2017) 209–221.
[55] J. Seo, L. Dueñas-Osorio, J.I. Craig, B.J. Goodno, Metamodel-based regional vulnerability estimate of irregular steel moment-frame structures subjected to earthquake events, Engineering Structures 45 (2012) 585–597.
[56] J.S. Jeon, A. Shafieezadeh, R. DesRoches, Statistical models for shear strength of RC beam-column joints using machine-learning techniques, Earthquake engineering & structural dynamics 43 (14) (2014) 2075–2095.
[57] S. Mangalathu, S.H. Hwang, J.S. Jeon, Failure mode and effects analysis of RC members based on machine-learning-based SHapley Additive exPlanations (SHAP) approach, Engineering Structures 219 (2020), 110927.
[58] Feng, D. C., & Fu, B. (2020). Shear strength of internal reinforced concrete beam-column joints: intelligent modeling approach and sensitivity analysis. Advances in Civil Engineering, 2020.
[59] D.C. Feng, B. Cetiner, M.R. Azadi Kakavand, E. Taciroglu, Data-driven approach to predict the plastic hinge length of reinforced concrete columns and its application, Journal of Structural Engineering 147 (2) (2021) 04020332.
[60] D.C. Feng, W.J. Wang, S. Mangalathu, E. Taciroglu, Interpretable XGBoost-SHAP machine-learning model for shear strength prediction of squat RC walls, Journal of Structural Engineering 147 (11) (2021) 04021173.
[61] X. Guan, H. Burton, M. Shokrabadi, Z. Yi, Seismic Drift Demand Estimation for Steel Moment Frame Buildings: From Mechanics-Based to Data-Driven Models, Journal of Structural Engineering 147 (6) (2021) 04021058.
[62] R.K. Mazumder, A.M. Salman, Y. Li, Failure risk analysis of pipelines using data-driven machine learning algorithms, Structural Safety 89 (2021), 102047.
[63] M.Z. Naser, S. Thai, H.T. Thai, Evaluating structural response of concrete-filled steel tubular columns through machine learning, Journal of Building Engineering 34 (2021), 101888.
[64] M. Zarringol, H.T. Thai, M.Z. Naser, Application of machine learning models for designing CFCFST columns, Journal of Constructional Steel Research 185 (2021), 106856.
[65] S. Mangalathu, J.S. Jeon, Machine learning–based failure mode recognition of circular reinforced concrete bridge columns: Comparative study, Journal of Structural Engineering 145 (10) (2019) 04019104.
[66] V.K. Kodur, M.Z. Naser, Classifying bridges for the risk of fire hazard via competitive machine learning, Advances in Bridge Engineering 2 (1) (2021) 1–12.
[67] S. Mangalathu, H. Sun, C.C. Nweke, Z. Yi, H.V. Burton, Classifying earthquake damage to buildings using machine learning, Earthquake Spectra 36 (1) (2020) 183–208.
[68] S. Mangalathu, J.S. Jeon, Classification of failure mode and prediction of shear strength for reinforced concrete beam-column joints using machine learning techniques, Engineering Structures 160 (2018) 85–94.
[69] B. Keshtegar, M.L. Nehdi, R. Kolahchi, N.T. Trung, M. Bagheri, Novel hybrid machine leaning model for predicting shear strength of reinforced concrete shear walls, Engineering with Computers (2021) 1–12.
[70] S. Mangalathu, H. Jang, S.H. Hwang, J.S. Jeon, Data-driven machine-learning-based seismic failure mode identification of reinforced concrete shear walls, Engineering Structures 208 (2020), 110331.
[71] V.L. Tran, D.K. Thai, S.E. Kim, Application of ANN in predicting ACC of SCFST column, Composite Structures 228 (2019), 111332.
[72] V.L. Tran, D.K. Thai, D.D. Nguyen, Practical artificial neural network tool for predicting the axial compression capacity of circular concrete-filled steel tube columns with ultra-high-strength concrete, Thin-Walled Structures 151 (2020), 106720.
[73] Zarringol, M., Thai, H. T., Thai, S., & Patel, V. (2020, December). Application of ANN to the design of CFST columns. In Structures (Vol. 28, pp. 2203-2220). Elsevier.
[74] S. Lee, T.P. Vo, H.T. Thai, J. Lee, V. Patel, Strength prediction of concrete-filled steel tubular columns using Categorical Gradient Boosting algorithm, Engineering Structures 238 (2021), 112109.
[75] Q.V. Vu, V.H. Truong, H.T. Thai, Machine learning-based prediction of CFST columns using gradient tree boosting algorithm, Composite Structures 259 (2021), 113505.
[76] F.Y. Liao, L.H. Han, Z. Tao, Behaviour of CFST stub columns with initial concrete imperfection: analysis and calculations, Thin-Walled Structures 70 (2013) 57–69.
[77] Z. Tao, Z.B. Wang, Q. Yu, Finite element modelling of concrete-filled steel stub columns under axial compression, Journal of constructional steel research 89 (2013) 121–131.
[78] D.C. Howell, Statistical methods for psychology, 7th Ed., Wadsworth, Cengage Learning, 2010.
[79] E. Al Daoud, Comparison between XGBoost, LightGBM and CatBoost using a home credit dataset, International Journal of Computer and Information Engineering 13 (1) (2019) 6–10.
[80] Chen, T., & Guestrin, C. (2016, August). Xgboost: A scalable tree boosting system. In Proceedings of the 22nd acm sigkdd international conference on knowledge discovery and data mining (pp. 785-794).
[81] G. Ke, Q. Meng, T. Finley, T. Wang, W. Chen, W. Ma, Q. Ye, T.Y. Liu, Lightgbm: A highly efficient gradient boosting decision tree, Advances in neural information processing systems 30 (2017) 3146–3154.
[82] Dorogush, A. V., Ershov, V., & Gulin, A. (2018). CatBoost: gradient boosting with categorical features support. arXiv preprint arXiv:1810.11363.
[83] F. Fu, Fire induced progressive collapse potential assessment of steel framed buildings using machine learning, Journal of Constructional Steel Research 166 (2020), 105918.
[84] J. Rahman, K.S. Ahmed, N.I. Khan, K. Islam, S. Mangalathu, Data-driven shear strength prediction of steel fiber reinforced concrete beams using machine learning approach, Engineering Structures 233 (2021), 111743.
[85] Nguyen, Q. H., Ly, H. B., Ho, L. S., Al-Ansari, N., Le, H. V., Tran, V. Q., Prakash, I. & Pham, B. T. (2021). Influence of data splitting on performance of machine learning models in prediction of shear strength of soil. Mathematical Problems in Engineering, 2021.
[86] T. Hastie, R. Tibshirani, J.H. Friedman, J.H. Friedman, The elements of statistical learning: data mining, inference, and prediction Vol. 2 (2009) 1–758.
[87] M.K. Ravindra, T.V. Galambos, Load and resistance factor design for steel, Journal of the Structural Division 104 (9) (1978) 1337–1353.
[88] K.C. Sener, A.H. Varma, Steel-plate composite walls: Experimental database and design for out-of-plane shear, Journal of Constructional Steel Research 100 (2014) 197–210.
[89] ASCE. (2017). "Minimum design loads for buildings and other structures." ASCE 7-16, Reston, VA.
[90] H.T. Thai, S. Thai, T. Ngo, B. Uy, W.H. Kang, S.J. Hicks, Reliability considerations of modern design codes for CFST columns, Journal of Constructional Steel Research 177 (2021), 106482.